# Experimental and numerical insights on the diagonal compression test for the shear characterisation of masonry

Jorge Segura[a,*], Luca Pelà[a], Savvas Saloustros[a], Pere Roca[a]

[a] Department of Civil and Environmental Engineering, Universitat Politècnica de Catalunya (UPC-BarcelonaTech), 08034 Barcelona, Spain

* Corresponding author. Department of Civil and Environmental Engineering, Universitat Politècnica de Catalunya (UPC-BarcelonaTech), Jordi Girona 1-3, 08034 Barcelona, Spain. E-mail address: jorge.segura@upc.edu

*Abstract:* The masonry tensile strength and shear modulus play a key role in the definition of the shear capacity of masonry structures. These properties are often determined experimentally by means of the diagonal compression test on square walls, which is regulated by the ASTM E519 standard. In spite of its wide use, the interpretation of the test is still controversial and no universal criterion exists on how to derive the masonry mechanical properties from the wall overall strength. Aiming to contribute in the improvement of the test's reliability and interpretation, this paper presents an investigation on the use of the diagonal compression test to characterize the shear properties of masonry. First, an experimental campaign on brickwork walls is described. The walls were built in laboratory in Flemish bond, a pattern that has been scarcely investigated in the available research studies on this type of test. Second, an advanced numerical model is used for the analysis of walls subjected to the diagonal compression test. The adopted numerical model, enhanced by a crack-tracking algorithm to reproduce accurately the tensile damage localization, constitutes a very useful and powerful tool to interpret correctly the behaviour during the test. Finite element analysis was executed to interpret the walls' response in the linear and nonlinear ranges with models properly calibrated by comparison with the experimental results. As a result, a criterion was determined for the

calculation of the tensile strength from the outcomes of the diagonal compression test. A sensitivity analysis was carried out with regard to the most influent material properties of the material, the geometrical dimensions of the panel, and the loading conditions of the testing setup. The findings of this research were finally applied and validated by means of simulations of diagonal compression tests from eight experimental campaigns performed by other authors on different masonry typologies.

*Keywords:* masonry, hydraulic lime, clay brick, tensile strength, shear modulus, diagonal compression test, macromodelling, crack-tracking, crack localization

*Highlights:*

- Diagonal compression tests on double-wythe Flemish bond masonry walls are presented
- Simulation of the diagonal compression test with an enhanced continuum FE model
- The diagonal compression test is interpreted in the linear and nonlinear range
- A coefficient of 0.4 is found adequate to compute the tensile strength of masonry
- The coefficient shows little sensitivity to panel size and size of loading shoes

## Nomenclature

| | |
|---|---|
| $A$ | net area of masonry specimen |
| $b$ | coefficient that accounts for the distribution of stresses within a wall |
| $c$ | cohesion |
| $d^{\pm}$ | tensile and compressive damage indexes |
| $CV$ | coefficient of variation |
| $E$ | Young's modulus |
| $f_{b,c}$ | compressive strength of bricks |
| $f_{b,f}$ | flexural tensile strength of bricks |
| $f_{b,sp}$ | indirect splitting strength of bricks |
| $f_c$ | compressive strength of masonry |
| $f_{m,c}$ | compressive strength of mortar |
| $f_{m,DPT}$ | compressive strength of mortar obtained through double punch tests |
| $f_{m,f}$ | flexural tensile strength of mortar |
| $f_t$ | tensile strength of masonry |
| $G$ | elastic shear modulus |
| $G_{fc}$ | compressive fracture energy of masonry |
| $G_{ft}$ | tensile fracture energy of masonry |

| | |
|---|---|
| $h$ | height of masonry specimen |
| $P$ | diagonal load |
| $P_{max}$ | maximum diagonal load |
| $t$ | thickness of masonry specimen |
| $w$ | width of masonry specimen |
| $\alpha_j$ | coefficient that modifies the quotient P/A to obtain the *j* stress component, normalized stress |
| $\alpha_{I,calc}$ | back-calculated coefficient that relates the maximum load to the tensile strength |
| $\gamma$ | shear strain |
| $\Delta$ | increase |
| $\delta$ | imposed displacement |
| $\varepsilon_c$ | compressive strain along compressed diagonal |
| $\varepsilon_t$ | tensile strain along compressed diagonal |
| $\sigma$ | normal stress |
| $\sigma_x$ | normal stress along X axis |
| $\sigma_y$ | normal stress along Y axis |
| $\sigma_I$ | maximum principal stress |
| $\sigma_{II}$ | minimum principal stress |
| $\sigma_0$ | compressive stress due to vertical loading |
| $\tau_m$ | average shear stress at failure |
| $\tau_{xy}$ | shear stress |
| $\Phi$ | internal angle of friction |
| $_{ASTM}$ | subscript for parameters obtained according to ASTM approach |
| $_{Frocht}$ | subscript for parameters obtained according to Frocht's approach |

# 1 Introduction

Shear walls resist the seismic effects in masonry buildings mostly through in-plane resisting modes. When local out-of-plane wall failures are prevented by appropriate connections between elements, the resisting mechanism that governs the global behaviour of the structure is the in-plane shear capacity of the walls [1,2], which is directly associated with the masonry shear strength.

The definition of the shear strength of masonry is not univocal [3]. Because of its complex and composite behaviour, masonry may experience different failure modes under lateral loading, depending on the relative mechanical properties of the constituents, the boundary conditions, the geometry, and the level of vertical load acting on the structure. Three mechanisms are usually identified as potential failure modes in shear [4]: a) rocking failure involving the overturning of the

wall and crushing of the compressed corner, b) shear sliding failure along a horizontal crack in the mortar bed-joints, and c) shear diagonal cracking through bed- and head-joints or also through the units. Different physical models have been adopted to estimate the shear capacity associated to the former mechanisms [3].

In the case of diagonal cracking, which is a recurrent mode observed after past earthquakes [3,5], Turnšek and Čačovič proposed a criterion that predicts the shear capacity of a wall for a given level of compressive stresses [6]. The criterion is based on a triple assumption: a) masonry is considered a homogeneous and isotropic material, b) failure occurs when the maximum principal stresses at the centre of the panel, which can be derived through the Mohr's circle from the acting shear and compressive stresses, exceed a reference value, and c) the reference value is supposed to be constant for walls made of the same material and represents a characteristic property of the material. Turnšek and Čačovič validated these assumptions experimentally and provided the following Equation 1 for the shear interaction diagram of a wall (presented herein in the more general form published in [7]):

$$\tau_m = \frac{f_t}{b}\sqrt{1+\frac{\sigma_0}{f_t}} \tag{1}$$

where $\tau_m$ and $\sigma_0$ are the average shear stress at failure and the compressive stress in the wall due to vertical loading respectively, and $b$ is a coefficient that accounts for the distribution of stresses within the panel. $f_t$ is the reference limit strength, defined and adopted as the conventional tensile strength of masonry [3,4]. Although the initial assumptions are drastic [4,8], this criterion is thoroughly diffused [9] as it manages to describe a complex behaviour with a single global parameter. Furthermore, the hypothesis of homogeneity is consistent with the continuum homogeneous models still in use for the analysis of masonry structures [8,10].

The experimental determination of this tensile strength of masonry would require the performance of shear-compression tests in the laboratory and the derivation of $f_t$ from the inverse of

Equation 1. These tests are however costly in terms of time and equipment as special loading apparatus are necessary to impose the proper boundary conditions and loads [11], and the mode of failure is difficult to control [5]. An alternative test that induces a state of stresses leading to a diagonal cracking failure is the diagonal compression test [1,7,12]. This type of test is considered to be more versatile, simpler, and less expensive [13–15].

The diagonal compression test consists of loading a masonry assemblage in compression along one of the diagonals, thus causing a tension failure with the specimen splitting apart parallel to the direction of load [16]. Given its ability to induce a shear diagonal cracking, it has been extensively used as a tool for comparing reinforcement products and techniques [5,17–21], as well as to investigate the mechanical behaviour of masonry in historical buildings [22–24]. This test is also recommended as a characterisation tool by several national and international building codes [25–27].

The American standard ASTM E519 [16] is the main reference that provides guidance on the features of the masonry specimens required for the test and on the loading conditions and protocols. It regulates the calculation of the acting stresses and the shear modulus of masonry as well. Based on the hypothesis of an isotropic linearly elastic material, the standard assumes a stress state of pure shear at the centre of the panel. Figure 1b represents the corresponding Mohr's circle, according to the coordinate system defined in Figure 1a. Under the hypothesis of pure shear, the maximum principal stress, $\sigma_I$, is equal to the shear stress, $\tau_{xy}$, and the standard proposes the following Equation 2 for their calculation:

$$\sigma_{I,ASTM} = \tau_{xy,ASTM} = 0.707\frac{P}{A} \tag{2}$$

where $P$ is the diagonal load at a given time and $A$ is the net area of the specimen computed with Equation 3:

$$A = t\frac{w+h}{2} \tag{3}$$

where $w$, $h$ and $t$ are the width, height and thickness of the specimen respectively. Equation 4 applies for the calculation of the tensile strength assuming that it is equal to the maximum principal stress at failure:

$$f_{t,ASTM} = 0.707\frac{P_{max}}{A} \tag{4}$$

where $P_{max}$ is the diagonal load value at failure. Additionally, there exists a recommendation by RILEM, LUMB6 [28], that covers also this test and specifies dimensions of specimens and apparatus. The suggested expression to calculate the tensile strength is the same as in ASTM E519 [16].

In 1931, Frocht found that a square plate made of an elastic isotropic material loaded in diagonal compression does not experience a pure shear state of stresses but a complex non-uniform one, where the normal components are not null [29]. Frocht drew this conclusion both from analytical derivation and by photoelasticity. These findings were confirmed afterwards in several instances by means of modern numerical methods [30–32]. Equations 5 to 7 show the expressions to calculate the acting stresses following Frocht's approach. Equation 8 relates the tensile strength of masonry with the maximum principal stress at failure:

$$\sigma_{x,Frocht} = \sigma_{y,Frocht} = -0.58\frac{P}{A} \tag{5}$$

$$\tau_{xy,Frocht} = 1.1\frac{P}{A} \tag{6}$$

$$\sigma_{I,Frocht} = 0.52\frac{P}{A} \tag{7}$$

$$f_{t,Frocht} = 0.52\frac{P_{max}}{A} \tag{8}$$

where $\sigma_x$ and $\sigma_y$ are the normal stresses. Figure 1c depicts the corresponding Mohr's circle. More recently, Brignola et al. [31] performed non-linear numerical analysis that accounted for the redistribution of stresses after failure and proposed new coefficients for Equation 8.

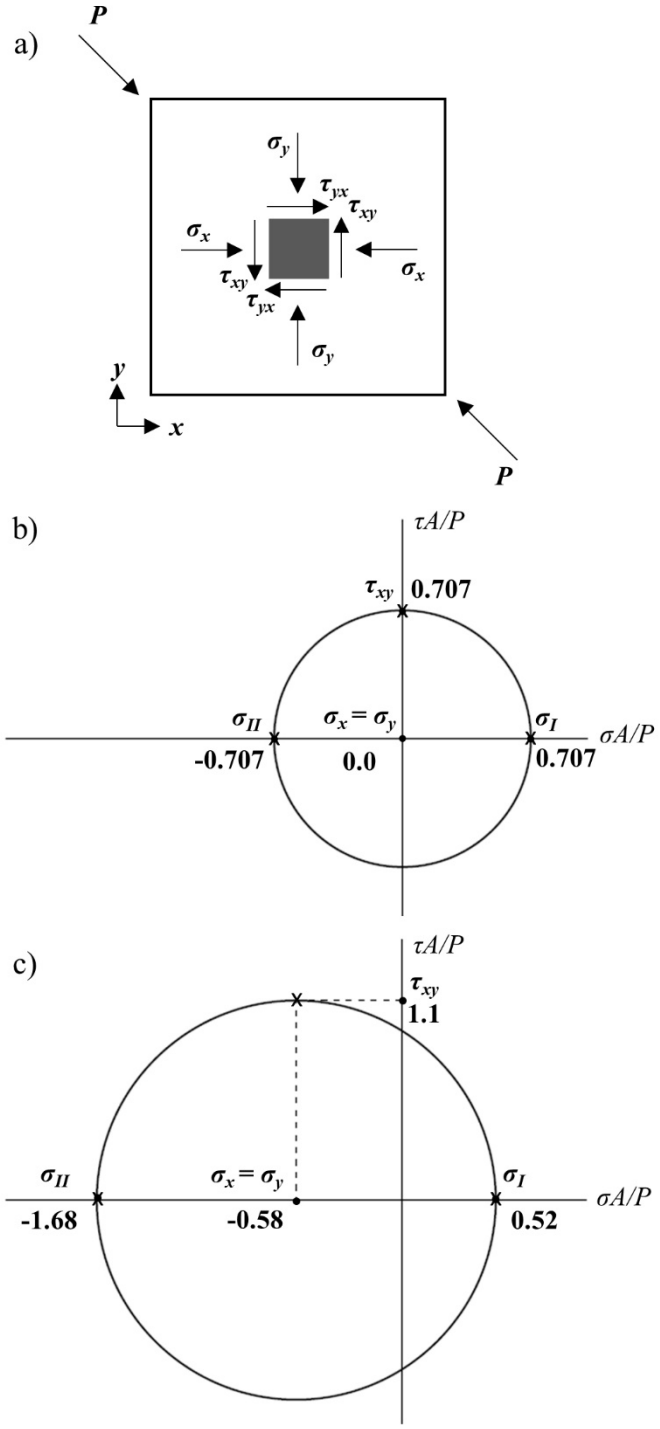


**Figure 1** a) Coordinate system in the diagonal compressed wall. b) Mohr's circle representations of the stresses at the centre of the panel according to ASTM's and c) Frocht's approaches.

As illustrated in Figure 1, both approaches, i.e. ASTM's and Frocht's, lead to different estimations of the tensile strength of masonry, but also of the acting shear stresses and the shear strength at zero compressive stress. Several authors have pointed out the controversy around these interpretations of the diagonal tests and have questioned the proposed formulae [1,11,13,22,33]. This

open debate hinders the applicability of the test and makes the comparison between researches difficult. Yet, even if the approach of ASTM E519 [16] overestimates the values of tensile strength compared to Frocht's approach, it is still the most spread standard, and Equation 2 is widely used [18–21,32,34–38].

The work presented herein provides new insights on the mechanical behaviour of masonry panels under diagonal compression, and investigates the use of this test for the determination of homogenised properties of masonry, specifically the tensile strength and the shear modulus.

The paper starts with two preliminary sections that describe the data and tools used to carry out the investigation. Section 2 presents an experimental campaign involving diagonal compression tests that will be used as calibration results. This campaign has additional relevance as it deals with tests on masonry walls made of clay bricks and hydraulic lime mortar arranged in Flemish bond. This masonry typology has received little attention until now in the available scientific literature [39], and its investigation constitutes a novel contribution of the paper. Section 3 describes the numerical tools used for the simulation of the experimental tests. The employed numerical model is based on a standard finite element formulation and includes the accurate description of tensile crack localization through a crack-tracking algorithm.

Section 4 constitutes the core of the paper. It includes the calibration of a numerical continuum model with the experiments of Section 2, the interpretation of the stress field within a masonry panel and the proposal of coefficients for the calculation of both the tensile strength and the shear modulus from diagonal tests. It also includes a sensitivity analysis of the proposed coefficients and their validation with cases investigated by other authors. Section 5 presents the concluding remarks of the research.

## 2 Experimental programme

The experimental programme presented herein had two main objectives: a) to provide experimental data to calibrate the numerical models necessary for the interpretation of the diagonal test, and b) to characterize a masonry typology recurrent in existing historical buildings. This section describes briefly the programme, which was carried out at the Laboratory of Technology of Structures and Building Materials of the Technical University of Catalonia (UPC – BarcelonaTech).

### 2.1 Materials

The masonry walls were built with handmade solid clay bricks and a low mechanical performance lime mortar, aiming to replicate a historical brickwork.

Solid clay bricks, moulded and fired manually, were provided by a local company. Bricks had average dimensions of 311 (length) × 149 (width) × 45 (height) mm³ and presented rough surfaces because of their traditional manufacturing. Table 1 includes the results of characterisation tests. The brick compressive strength, $f_{b,c}$, was estimated according to the standard EN 772-1 [40] on cut pieces of 100 × 100 mm². Two different types of test were carried out to approximate the tensile strength of the bricks: three-point-bending tests on full bricks according to EN 772-6 [41] to evaluate the flexural tensile strength, $f_{b,f}$, and Brazilian tests on prismatic pieces of 160 × 40 × 40 mm³ to estimate the indirect splitting tensile strength, $f_{b,sp}$.

A hydraulic lime based commercial mortar was chosen as binding material. This mortar was modified with limestone filler additions to reduce its strength, as explained by the authors in a recent publication [42]. During the construction of each masonry wall, mortar prisms with dimensions 160 × 40 × 40 mm³ were prepared from the mason's batch. Each set of prisms was tested at the same time of its companion wall. Table 1 presents the average compressive strength, $f_{m,c}$, and the average flexural tensile strength, $f_{m,f}$, of mortar determined according to EN 1015-11 [43]. Additionally, after the test of each wall, some masonry bed-joints were disassembled with the aim of extracting mortar samples to perform double-punch tests (DPT). Specimens with approximated dimensions of 50 × 50 × 15 mm³ were tested according to DIN 18555-9 [44] to assess the mortar compressive strength within the joints,

$f_{m,DPT}$. The difference between the compressive strength values estimated from prisms and extracted joints can be explained, according to recent researches, by the differences in thickness and curing conditions of the specimens, and by the different loading conditions specific of each type of test [45–48].

Masonry specimens made with these two same components were tested in parallel campaigns [49] to evaluate the compressive and shear mechanical properties of the masonry composite (see Table 1). The compressive strength of masonry, $f_c$, was obtained from tests on running bond walls according to EN 1052-1 [50]. Two additional tests on stack bond prisms provided estimations of the compressive fracture energy, $G_{fc}$, calculated as the area below the stress displacement curves through Riemann sums [49]. Triplet specimens were tested by following the standard EN 1052-3 [51] to determine the cohesion, $c$, and angle of friction, $\Phi$, of the masonry bed-joints. As recommended by the standard, three different compressive load levels were applied, with three triplet specimens for each level.

**Table 1** Mechanical properties of constituent materials (brick and mortar) and of masonry composite

| **Brick** | $f_{b,c}$ [MPa] | $f_{b,f}$ [MPa] | $f_{b,sp}$ [MPa] | |
|---|---|---|---|---|
| Average | 17.99 | 2.44 | 1.44 | |
| Number of specimens | 20 | 10 | 24 | |
| CV | 8.3% | 20.0% | 13.0% | |
| **Mortar** | $f_{m,c}$ [MPa] | $f_{m,f}$ [MPa] | $f_{m,DPT}$ [MPa] | |
| Average | 2.19 | 0.66 | 5.11 | |
| Number of specimens | 38 | 76 | 232 | |
| CV | 26.1% | 25.4% | 23.0% | |
| **Masonry*** | $f_c$ [MPa] | $G_{fc}$ [N/m] | $c$ [MPa] | $\Phi$ [°] |
| Average | 6.51 | 9750 | 0.16 | 33.71 |
| Number of specimens | 4 | 2 | 3x3 | 3x3 |
| CV | 8.9% | 15.2% | - | - |

* These properties were estimated in previous campaigns not included in this research [49]

## 2.2 Masonry specimens

Five double-leaf masonry walls with nominal dimensions 1270 × 1270 × 311 mm³ were built in the laboratory. The specimens were labelled URM_#, where # is a digit from 1 to 5. The chosen dimensions allowed to satisfy the geometrical requirements established in the standard ASTM E519 [16] and in the recommendations LUMB6 of RILEM [28], i.e. have a minimum dimension of 1200

mm and be a minimum of four units wide, respectively. The walls were built in Flemish bond, as shown in Figure 2. This bond pattern is particularly common in historical buildings [24,52] but still few experimental results are available in literature for this typology [24,39]. As reported in [5], there is a lack of experimental evidence on double-wythe masonry.

Professional bricklayers built the walls on metallic C-profiles. This measure facilitated the later handling of the specimens. To avoid any influence of the metallic base during the tests, an interface consisting of one Teflon sheet 3 mm thick and one PVC sheet 3 mm thick was placed on top of the C-profile before laying the first joint of mortar (see Figure 2). Up to 21 brick courses conformed the walls, with 15 mm thick mortar joints. This thickness was necessary to accommodate the irregularities of the brick surfaces. After the construction, the walls were stored in laboratory conditions during the curing of the mortar and were tested after 28 days.

### 2.3 Setup and testing procedure

The standard ASTM E519 [16] served as reference for the execution of the tests. However, a modification was introduced with respect to the positioning of the walls and they were kept horizontal instead of rotated 45 degrees. This measure avoided any damage during the handling of the specimens due to their low strength and is rather common in research practice [17,53,54]. Furthermore, this setup replicates the same one used for in-situ testing [22,23].

Figure 2 displays the entire experimental setup for testing a wall. The specimens were placed on top of a metallic bench. Two steel loading-shoes, bolted to two robust beams, were placed at two diagonally opposite corners of the specimens. The two beams were connected by two Dywidag bars, one at each face of the walls. During the test, two hydraulic jacks pulled the bars, thus creating a closed-loop system and introducing the diagonal load into the specimens [53]. The loading depth of the steel shoes at the corners was of 140 mm. The ratio of the loaded depth (140 mm) with respect to the total width of the wall (1270 mm) is equal to $1/9^{th}$. This ratio was chosen as a compromise between

the suggestions reported in ASTM E519 [16] and in RILEM LUMB6 [28], which are $1/8^{th}$ and $1/10^{th}$ respectively.

The loading protocol involved two stages, following the approach applied by the authors in [49]. The first stage aimed to facilitate the measurement of the elastic shear modulus of masonry, and consisted of the application of three loading-unloading cycles, from 10 to 50 kN under load control. These load levels were set to approximately 5% and 30% of a maximum load that had been estimated before the tests. The execution of cycles, as reported in [49] and suggested by specific standards for the determination of elastic properties (e.g. [55,56]), minimizes the possible errors due to initial effects of backlash and specimen irregularities. Cycles were not performed in the wall URM-2. The second stage of the tests investigated the ultimate capacity. The load was applied beyond failure under displacement control at a constant rate of approximately 0.5 mm/min. The tests were stopped when the reduction of the load attained approximately 50% of the registered peak load.

Besides the pressure transducer and the encoder necessary to control the hydraulic jacks, the walls were mainly instrumented with four linear variable differential transducers (LVDTs). The mounted instruments had a displacement range of ± 5 mm and a precision of 5 μm. Two LVDTs were placed on each face of the specimens along the diagonals, one aimed to measure the shortening of the compressed diagonal and the other aimed to capture the elongation of the diagonal under tension. Redundant instrumentation, including wire sensors and additional displacement transducers, was mounted to assess the global behaviour of the walls during the tests. Further details on the whole setup and testing procedure are available in [21,57], which covers a parallel research on strengthened masonry.

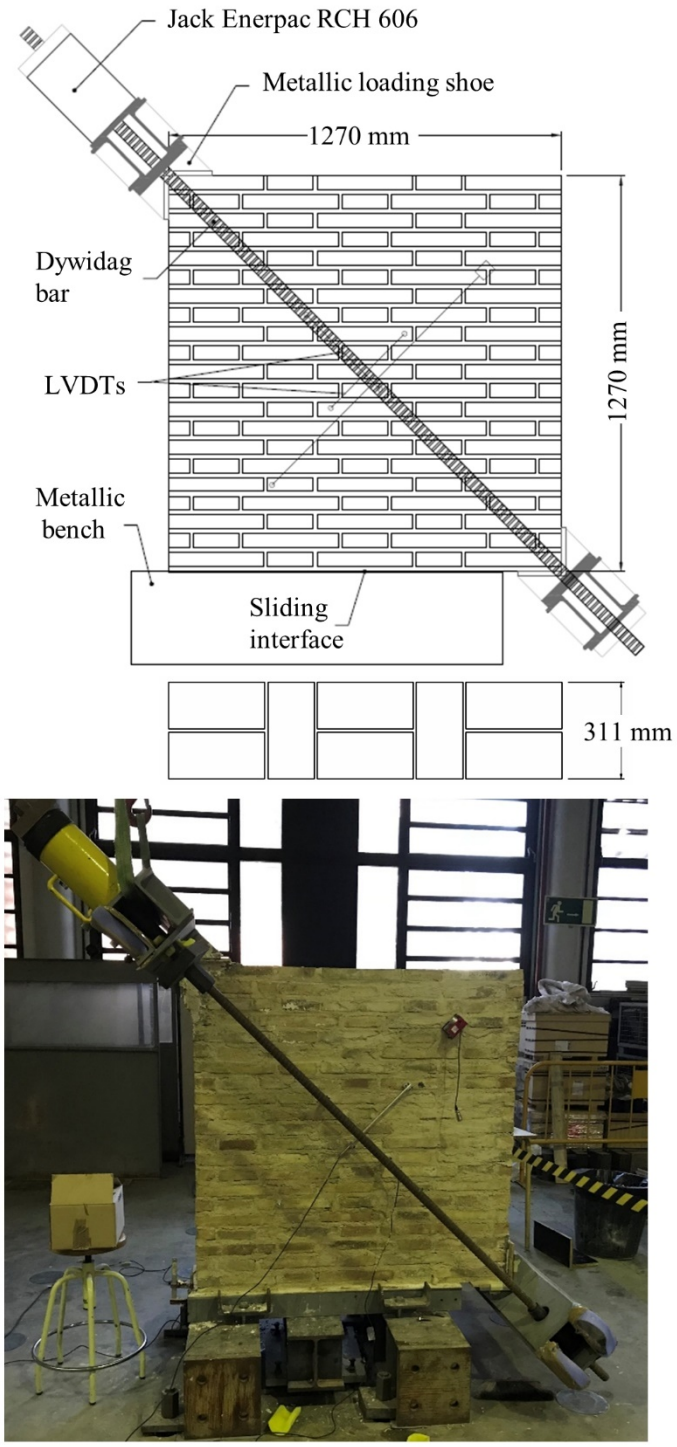


**Figure 2** Setup of the diagonal compression test.

After the tests, the tensile strengths of each wall were evaluated with Equations 4 and 8 corresponding to the different approaches of ASTM E519 [16] and Frocht [29]. The shear strains γ were calculated with the following Equation 9 [16]:

$$\gamma = \varepsilon_c + \varepsilon_t \tag{9}$$

where $\varepsilon_c$ and $\varepsilon_t$ are the compressive and tensile strains along the compressed and tensioned diagonals, obtained as the average of the readings from the LVDTs on both sides of the wall. The shear elastic moduli were evaluated as the chord modulus between the 5% and 30% of the actual maximum load ($P_{max}$) of the shear stress-strain curves. Equations 10 and 11 present the expressions to calculate the shear elastic moduli G for each of the considered approaches, where the shear stresses are evaluated with Equations 2 and 6:

$$G_{ASTM} = \frac{0.707 \frac{\Delta P_{5-30\%}}{A}}{\Delta \gamma_{5-30\%}} \tag{10}$$

$$G_{Frocht} = \frac{1.1 \frac{\Delta P_{5-30\%}}{A}}{\Delta \gamma_{5-30\%}} \tag{11}$$

where $\Delta P_{5\text{-}30\%}$ and $\Delta \gamma_{5\text{-}30\%}$ stand for the increase of load and strain respectively between the 5% and 30% of the maximum load.

**2.4 Experimental results**

Figure 3 displays the crack patterns of the five walls after failure. These patterns were qualitatively similar and, in all cases, a final diagonal main crack connected both loaded corners. The particularity of the Flemish bond used to build the walls reflects in the number of bricks affected by the crack. Contrarily to other bond arrangements such as header bond, where cracks follow the mortar joints and bricks are broken only rarely [17,58], the length of the bricks used herein hindered the formation of a stair-stepped crack and necessarily required the failure of bricks in tension. Figure 3f includes a detail of URM_2 that shows cracks involving both bricks and mortar joints.

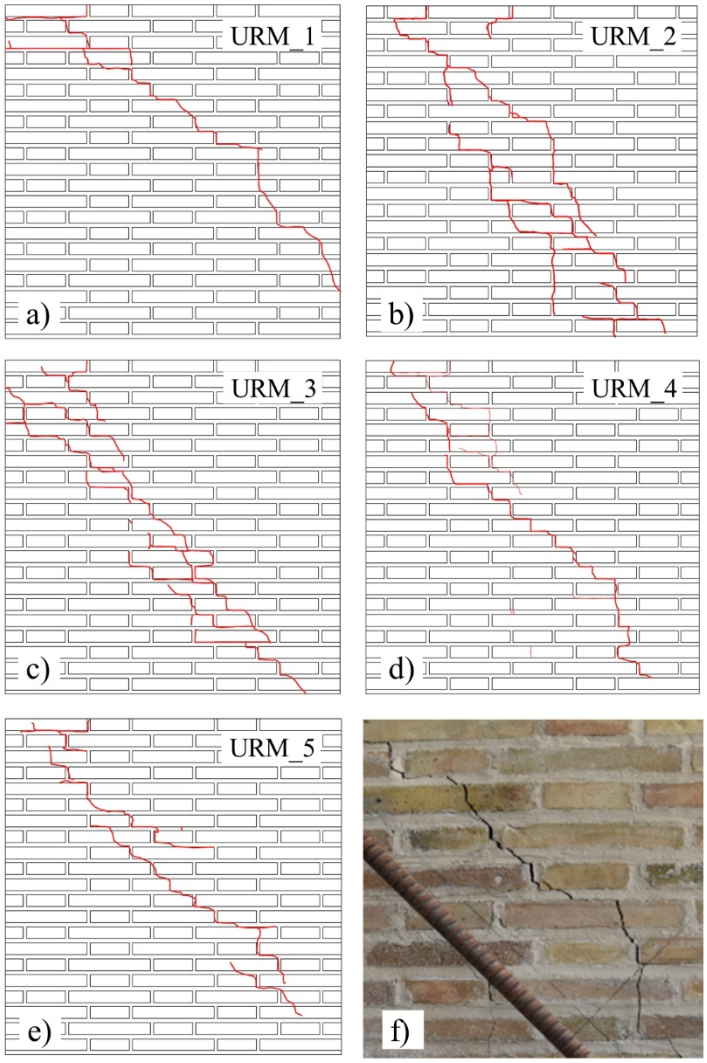


**Figure 3** a) to e) Crack patterns at the end of the test for the five specimens. f) Pattern detail of wall URM_2 with cracks involving both bricks and mortar joints.

Figure 4 displays two types of curves. Figure 4a depicts the load–displacement curves corresponding to the five walls, with the displacement corresponding to the shortening of the compressed diagonal measured with the encoder of the jacks. Figure 4b displays the load–strain curves of four walls, obtained from the readings of the LVDTs placed along the compressed and tensioned diagonals (URM_2 curves are not available due to premature detachment of sensors during the test). According to Figure 4a, the five walls presented a relatively brittle behaviour. In all cases, the load increased almost linearly with the imposed displacement until a sudden drop of the load occurred. The curves obtained with the LVDTs at the central zone of the specimen, presented in Figure 4b, show a change in the slope of the loading curves before the maximum load $P_{max}$. This change would indicate

the appearance of initial damage and was detected by both the LVDTs and the redundant instrumentation at a load level around 80 to 90% of the maximum load. At that moment, superficial cracks were not visible to the naked eye. Full cracks connecting the corners appeared at the maximum load or immediately after, and continued to develop and open during the loss of bearing capacity of the wall. The cracks involved the full thickness and were visible on both faces of the walls. The opening of the central diagonal cracks affected clearly the readings of the LVDTs. Only in the case of specimen URM_3, cracks started clearly at the centre of the panel and progressed along the diagonal to reach the corners. In the rest of specimens, it was difficult to identify the starting point of cracks, as they appeared almost simultaneously along the full length.

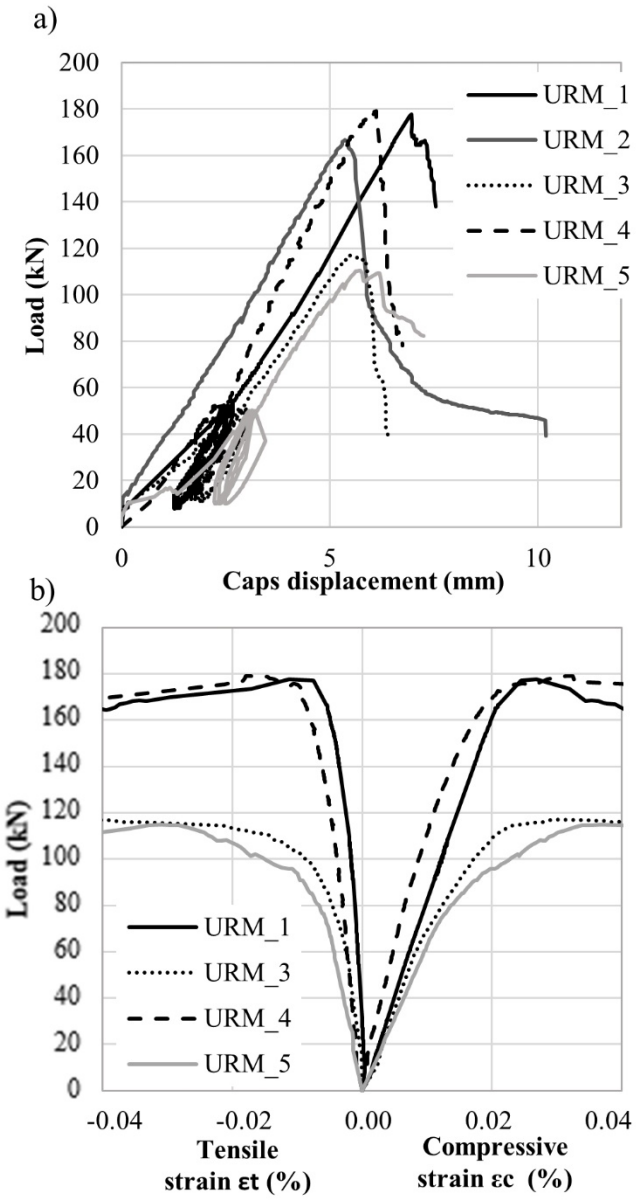


**Figure 4** a) Load – displacement curves for the five walls, including the initial loading-unloading cycles, the peak load and the loss of capacity after failure.. b) Load – strain curves for four walls, measured with the LVDTs placed along the compressed and tensioned diagonals. The initial loading-unloading cycles are not shown. No strain curves are given for specimen URM_2 due to detachment of the LVDTs during the test.

Table 2 presents a summary of the experimental results from diagonal compression tests on the five walls. Table 2 indicates the registered values of maximum load $P_{max}$ and the calculated values of tensile strength $f_t$ and shear modulus $G$ according to the two approaches and Equations 4, 8, 10 and 11. No values of shear modulus are given for specimen URM_2 due to invalid readings of the LVDTs during the test. The need of delving into the interpretation of the diagonal test outcomes is evident in the light of the obtained average results. Compared to the standard procedure of the ASTM E519 [16],

the estimations of the tensile strength and shear modulus of masonry with Frocht's approach are 36% lower and 56% higher respectively.

**Table 2** Experimental results. Maximum load, tensile strength and shear modulus of each specimen

| Specimen | $P_{max}$ [kN] | $f_{t,ASTM}$ [MPa] | $f_{t,Frocht}$ [MPa] | $G_{ASTM}$ [MPa] | $G_{Frocht}$ [MPa] |
|---|---|---|---|---|---|
| URM_1 | 178 | 0.32 | 0.24 | 1536 | 2389 |
| URM_2 | 167 | 0.30 | 0.22 | - | - |
| URM_3 | 117 | 0.21 | 0.15 | 1149 | 1787 |
| URM_4 | 179 | 0.32 | 0.23 | 1571 | 2444 |
| URM_5 | 115 | 0.21 | 0.15 | 883 | 1375 |
| Average | 151 | 0.27 | 0.20 | 1285 | 1999 |
| St. Dev. | 32 | 0.06 | 0.04 | 329 | 512 |
| CV | 21.5% | 21.3% | 21.3% | 25.6% | 25.6% |

The coefficients of variation of the experimental results range from 20 to 25%. This relatively high variability is common in this type of material and typology of test [1,19,32,59]. According to the coefficients of variation presented for bricks and mortar in Table 1, the inherent variability of the material constituents can fully explain the scattering found in the diagonal compression tests. In this type of tests, cracks are localized in a narrow band of the wall, as shown in Figure 3. Given the brittleness of the observed failures, and in agreement with the weakest-link postulate for brittle materials [60], it could be expected that the global results were sensitive to the local properties of the constituents. Another additional source of variability is given by the Flemish bond and the relevant two-brick thickness of the walls, which constitutes a further complexity in the material structure compared with the recurrent tests available in the literature on one brick walls with units laid in a stretcher pattern.

As will be seen in section 4.1, this variability is helpful to the aim of this study because the results can be grouped in data sets of similar properties, and they can be used for the calibration of the numerical model in Section 4. Table 3 identifies the three proposed data sets, one corresponding to the average values and the other two corresponding to the higher and lower values.

**Table 3** Experimental data sets for numerical calibration

| Data set | Specimens | $P_{max}$ [kN] | $f_{t,ASTM}$ [MPa] | $f_{t,Frocht}$ [MPa] | $G_{ASTM}$ [MPa] | $G_{Frocht}$ [MPa] |
|---|---|---|---|---|---|---|

| | | | | | | |
|---|---|---|---|---|---|---|
| High-set | URM 1 & 4 | 178.5 | 0.32 | 0.23 | 1553 | 2417 |
| Average-set | URM 1 to 5 | 151 | 0.27 | 0.20 | 1285 | 1999 |
| Low-set | URM 3 & 5 | 116 | 0.21 | 0.15 | 1016 | 1580 |

# 3 Numerical tools

This section 3 provides the details of the numerical model employed in Section 4 to interpret the diagonal compression tests. Section 3.1 presents the modelling approach, Section 3.2 provides a brief description of the constitutive model used for the materials, and Section 3.3. reports details on the simulation process.

## 3.1 Modelling approach

Different approaches have been adopted in recent years for the numerical simulation of diagonal compression tests. The possibilities span from distinct element models [61] to continuous finite element models, the latter covering a variety of cases depending on the level of discretisation detail: 3D and 2D homogeneous macromodels with a single masonry material [14,61,62], 3D and 2D simplified micromodels with no unit-joint interfaces [63,64], micromodels with simplified interfaces [65], or detailed micromodels [66], with diverse options of material constitutive laws.

This research investigates the use of the diagonal compression test to determine homogenised mechanical properties of masonry considered as a continuous isotropic material. Consistently, a macromodelling approach has been applied to simulate the tests. With this approach, only two materials are considered: steel for the loading shoes, and masonry as a homogeneous material for the wall. This strategy allows a direct comparison between the experimental outcomes and the material input parameters within the same framework. It is also coherent with Section 1 and the initial hypothesis of homogeneity and isotropy on which Turnšek and Čačovič based their criterion [6].

## 3.2 Constitutive model

The nonlinear behaviour of the masonry material is modelled with a constitutive model based on Continuum-Damage Mechanics [67]. For the sake of simplicity, few aspects are highlighted in the following. The reader is referred to the most recent developments on the model for further details [68].

The strain-based continuum damage model uses two scalar damage variables that allow to distinguish between tensile ($d^+$) and compressive ($d^-$) damage. The constitutive law is given in Equation 12:

$$\boldsymbol{\sigma} = (1 - d^+)\bar{\boldsymbol{\sigma}}^+ + (1 - d^-)\bar{\boldsymbol{\sigma}}^- \tag{12}$$

where $\boldsymbol{\sigma}$ is the stress tensor, and the effective stress tensor $\bar{\boldsymbol{\sigma}}$ is split in a tensor related to tension stress states $\bar{\boldsymbol{\sigma}}^+$and in a tensor related to compression stress states $\bar{\boldsymbol{\sigma}}^-$.

Two additional scalar variables, $\tau^{\pm}$, the equivalent stresses, determine the shape of the positive and negative damage surfaces, expressed according to Equations 13 and 14:

$$\tau^+ = H[\bar{\sigma}_{max}]\frac{1}{1-a}\left[\sqrt{3\bar{J}_2} + a\bar{I}_1 + b\langle\bar{\sigma}_{max}\rangle\right]\frac{f^+}{f^-} \tag{13}$$

$$\tau^- = H[-\bar{\sigma}_{min}]\frac{1}{1-a}\left[\sqrt{3\bar{J}_2} + a\bar{I}_1 + \kappa_1 b\langle\bar{\sigma}_{max}\rangle\right] \tag{14}$$

with

$$a = \frac{(f_b^-/f^-) - 1}{2(f_b^-/f^-) - 1} \tag{15}$$

$$b = (1-a)\frac{f^-}{f^+} - (1+a) \tag{16}$$

In the above, $\bar{I}_1$ is the first invariant of the effective stress tensor and $\bar{J}_2$the second invariant of the deviatoric effective stress tensor. $f^+$ and $f^-$ stand for the tensile and compressive strengths respectively and $f_b^-$ for the biaxial compressive strength. $\bar{\sigma}_{max}$ and $\bar{\sigma}_{min}$ denote the maximum and minimum principal effective stresses respectively. $H$[x] is the Heaviside step function and the symbols $\langle\cdot\rangle$ are the Macaulay brackets ($\langle x\rangle = x, if\ x \geq 0, \langle x\rangle = 0, if\ x < 0$).

The failure surfaces described above stand for a tension-compression damage model. Within a wall subjected to diagonal compression, the combination of tension and compression leads to a shear

stress state. The parameter $\kappa_1$ introduced in Equation 14 is a constant proposed by Petracca et al. [69,70] for an enhanced mechanical description of the shear behaviour of masonry structures, as it controls the shape of the failure surface in the shear quadrants. Note that a zero value of $\kappa_1$ leads to the Drucker-Prager criterion, while a unity value yields a criterion equivalent to the one proposed by Lubliner et al. [71]. Petracca et al. [69,70] have obtained satisfactory results in simulations of shear loading and diagonal cracking when using this model.

The basis of the model also includes the definition of internal variables for the representation of the current damage thresholds, as well as the evolution laws for the damage variables. An exponential softening law is adopted in tension, while a parabolic hardening – exponential softening curve applies in compression. Six material properties are required to define the model input parameters [72]: both tensile, $f_t$, and compressive, $f_c$, strengths, both tensile, $G_{ft}$, and compressive, $G_{fc}$, fracture energies, and the elastic properties Young's modulus, $E$, and Poisson's ratio, $v$.

Additionally, the implementation of a local crack-tracking algorithm allows the simulation of localized cracks. This feature is especially convenient to the actual localized cracking found in the diagonal compression experiments, and provides a more realistic representation of the cracks if compared with the common smeared damage approach [73]. This algorithm identifies the elements crossed by propagating cracks at each time/load increment, see references [68,73–77] for further details and the latest developments on this numerical technique. The use of a nonlinear stress-strain relationship for the elements on the crack path, together with a linear elastic response for the ones outside, allows the simulation of discrete cracks. The parameters of the crack-tracking algorithm have already been calibrated with shear benchmark problems [68,77] and are directly implemented herein.

### 3.3 Numerical simulation

The diagonal compression test has been analysed under plane stress conditions. The simulation of the load application has been performed through imposed displacements, ($\delta_u$, $\delta_v$, see Figure 5a),

with increasing magnitude, in agreement with the testing procedure. Displacements of the same magnitude and opposite direction were imposed at both corners of the wall simultaneously. As shown in Figure 5a, simplified steel loading shoes have been included to better simulate the load application. The actual geometry of the masonry specimens is modelled with average dimensions.

The discretization of the specimens consists of an unstructured mesh of 2D plane-stress three-node triangles (see Figure 5b). The reference mesh contains 8573 nodes, with average mesh size, $h_e$, of 13 mm. Such a refined mesh aimed at a more accurate estimation of the stress levels in the centre of the specimen.

The choice of a suitable reference measurement for the comparison between experimental and numerical curves to calibrate the models constituted a crucial point of the study. The use of the overall stroke of the jacks, as shown in Figure 4a, compared to the displacement between corner nodes was not suitable due to spurious readings associated to initial deformations of the loading devices. The compressive strain shown in Figure 4b, computed from the experimental readings of the LVDTs placed along the compressed diagonal, was eventually chosen. This magnitude was compared to the numerical compressive strain calculated between two nodes of the compressed diagonal. These two nodes acted as a "virtual LVDT" placed at an equivalent position of the experimental LVDTs (see Figure 2 and Figure 5). However, the value of this compressive strain, immediately before and after the peak load, is affected in both the experimental case and numerical cases by the opening of the diagonal crack. Given the randomness of the experimental cracking, it was decided, during the calibration process, to focus on the comparison of the experimental and numerical initial stiffness and maximum load. This comparison allows the evaluation of the tensile strength and the shear modulus of masonry.

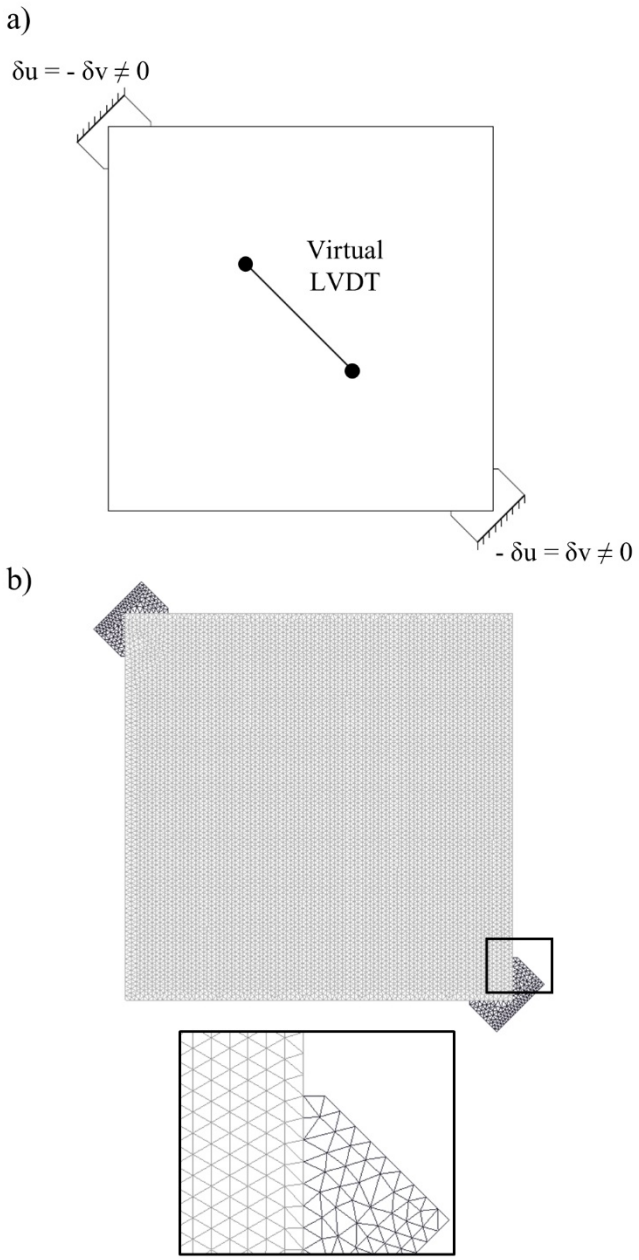


**Figure 5** a) Boundary conditions on the numerical simulation and position of the virtual LVDT for comparison. b) Discretized domain used for the macromodelling approach.

The numerical solution was carried out in an incremental manner. A modified Newton-Raphson method (using the secant stiffness matrix) together with a line-search procedure were used to solve the corresponding nonlinear equations. To achieve convergence at each step, the maximum value of the ratio between the norm of the iterative residual forces and the norm of the total external forces was set at $10^{-2}$. Calculations were performed with an enhanced version of the finite element software COMET [78], while the software GiD [79] was used for the pre- and post-processing of the model. Both

software have been developed at the International Centre for Numerical Methods in Engineering (CIMNE), in Barcelona.

# 4 Study on the use of the diagonal compression test to estimate homogenised properties of masonry

This section investigates the possibility of using the experimental outcomes of the diagonal compression test to determine two mechanical properties of masonry: tensile strength and shear modulus. The basic hypothesis is considering masonry as a homogeneous and isotropic material, in correspondence with the assumption of the Turnšek and Čačovič criterion. Thus, the tensile strength and shear modulus are considered as global and intrinsic parameters of the material.

The investigation begins with the calibration of a numerical macromodel with the experimental results exposed in Section 2. Once the model is calibrated, the state of stresses within a reference panel is interpreted, and a factor is proposed to calculate the tensile strength. A sensitivity analysis evaluates the influence on this factor of the input material properties, the panel size and the dimensions of the loaded corners. Eight different experimental campaigns available in the scientific literature have been used as benchmark problems to validate the findings of this section for different masonry typologies.

## 4.1 Calibration of the macromodel

The numerical macromodel has been calibrated to fit the experimental curves of the three data sets defined in Table 3. The calibration process followed a splitting approach, as defined by Chisari et al. [65]. The first stage involved the calibration of the elastic parameters, Young's modulus and Poisson's ratio, to adjust the slopes of the curves. The second stage required the calibration of the tensile strength and the tensile fracture energy to reach the corresponding maximum load.

The initial values of the mechanical properties were chosen as follows. The compressive strength and compressive fracture energy of masonry were always taken equal to the experimental

values provided in Table 1. The experimental shear moduli obtained from both approaches, i.e. ASTM's and Frocht's in Table 3, were used to determine the Young's moduli by means of the relationship $E = 2G(1 + v)$. Assuming an isotropic homogeneous material, the former expression is valid due the elastic linear behaviour presented by the walls at low load levels. Different values of Poisson's ratio were checked. The experimental values of tensile strength obtained from both approaches (Table 3) were assumed as starting point. Two different expressions were used to link the tensile fracture energy to the strength of masonry. Equation 17 was proposed by Angelillo et al. [80] as an adaptation from Model Code 1990 for concrete structures [81]. Equation 18 is the proposal of the Model Code 2010 [82].

$$G_{ft} = 0.04\, f_t^{0.7} \tag{17}$$

$$G_{ft} = 73\, f_c^{0.18} \tag{18}$$

Figure 6 shows the results of the calibration with the comparison between the numerical and the experimental curves. As explained in Section 3.3, the calibration is focused mainly in the initial slope and the maximum attained load. A direct comparison of the post-peak response is hindered by the influence of the location and crack opening in the readings of the LVDTs. Figure 7 displays the contour of maximum principal strains in the finite element model for one of the cases after failure. The resulting numerical crack is perfectly diagonal and mesh-independent, proving the high accuracy of the considered computational technique. The adopted numerical approach simulates well the described crack patterns obtained experimentally and shown in Figure 3. Table 4 includes the final input parameters for the three different data sets and the comparison between the numerical and experimental maximum loads. The difference is always lower than 2%.

Regarding the input data indicated in Table 4, the final values of Young's moduli, which best fitted the experimental slopes, corresponded to those obtained from the values of shear moduli given by Frocht's expression (Equation 6). The input tensile strength was the most relevant parameter affecting the appearance of damage and defining the maximum load. In the three data sets, the values

obtained by means of ASTM's and Frocht's approach (Equations 4 and 8) led to very high values of peak load. In the three data sets, in order to attain the sought load levels, it was necessary to reduce the input tensile strength to a value close to 0.40 times the experimental load $P_{exp}$ over the area $A$. The modified expression from Model Code 1990 for the tensile fracture energy (Equation 17) worked well also for the three data sets. These satisfactory results were obtained with a constant value of 0.16 for the numerical parameter κ1 proposed by Petracca et al. [69,70]. The same value was used in [68,70,83] to simulate other shear tests. The calibration process described in this paragraph applied for the three different data sets and led to good simulations of the initial slopes of the experimental curves, the maximum attained loads, and the failure mechanism.

**Table 4** Calibration of the numerical model with experimental results: Input data for the numerical analyses of the three data sets, and comparison between experimental and numerical maximum loads.

| | *Input data* | | | | | | | *Comparison exp - num* | | |
|---|---|---|---|---|---|---|---|---|---|---|
| *Data set* | $E$ (MPa) | $\nu$ (-) | $f_t$ (MPa) | $f_c$ (MPa) | $G_{ft}$ (N/m) | $G_{fc}$ (N/m) | $\kappa_1$ (-) | $P_{exp}$ (kN) | $P_{num}$ (kN) | $\Delta_{exp\text{-}num}$ |
| High-set | 4203 | 0.15 | 0.183 | 6.51 | 12.17 | 9750 | 0.16 | 178.5 | 176.3 | + 1.2% |
| Average-set | 3477 | 0.15 | 0.155 | 6.51 | 10.85 | 9750 | 0.16 | 151 | 151.8 | -0.5% |
| Low-set | 2748 | 0.15 | 0.119 | 6.51 | 9.03 | 9750 | 0.16 | 116 | 117.6 | -1.4% |

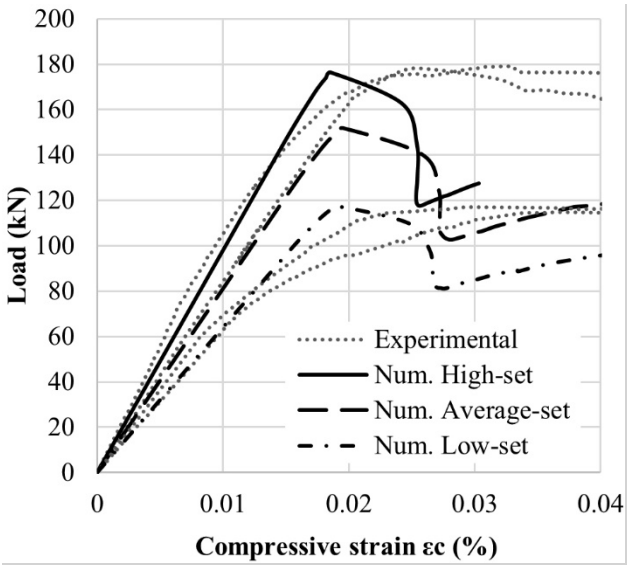


**Figure 6** Comparison between the load-strain curves of the experimental tests and the numerical analyses. No experimental curve is given for specimen URM_2 due to invalid readings of the LVDTs during the test.

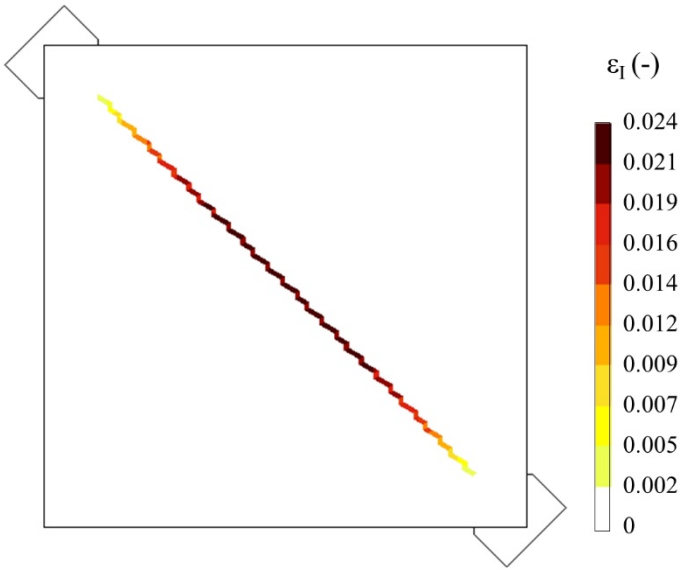


**Figure 7** Contour of the maximum principal strains, $\varepsilon_I$, after the peak load.

## 4.2 Interpretation of the diagonal test

The previous section allowed having a properly calibrated numerical model able to simulate satisfactorily the experimental diagonal compression tests. This section seeks to interpret the state of stresses within the panel and to derive conclusions on the use of the experimental outcomes to

determine mechanical properties of masonry. The average data set defined in Table 3 is used as a reference in the following.

### 4.2.1 Linear range

First, the focus is placed in the initial stage of the analysis when the wall still behaves linearly, i.e. without any damage. For the sake of clarity, it is decided to define a series of coefficients alpha $\alpha$ or normalized stresses for the different stress components, according to the applied load $P$ over the transversal section $A$. For a given time-step ($i$), the coefficients for the different stresses ($\sigma_x$, $\sigma_y$, $\tau_{xy}$, $\sigma_I$) are defined with Equations 19a to 19d:

$$\alpha_x(i) = \sigma_x(i)\frac{A}{P(i)} \tag{19a}$$

$$\alpha_y(i) = \sigma_y(i)\frac{A}{P(i)} \tag{19b}$$

$$\alpha_{xy}(i) = \sigma_{xy}(i)\frac{A}{P(i)} \tag{19c}$$

$$\alpha_I(i) = \sigma_I(i)\frac{A}{P(i)} \tag{19d}$$

Figure 8 shows three contour plots that represent the stress state of the wall in the linear range. The coefficient $\alpha$ corresponding to each stress component at the centre of the panel is indicated below each of the plots. Unlike the hypothesis of pure shear stated in the American standard ASTM E519 [16], Figure 8a illustrates that the normal stresses along the X-axis (also along Y-axis) are not null. As pointed out by Gabor et al. [64], the stress condition of pure shear would require an additional pair of tensile forces acting at the opposite free corners. The coefficients found in the research presented herein ($\alpha_x$ = -0.56, $\alpha_{xy}$ = 1.04, $\alpha_I$ = 0.48) are very similar to those found by Brignola et al. [31], and agree with the elastic solution proposed by Frocht [29]. The slight differences between the values obtained with numerical methods and those found by Frocht may be due to the consideration of Poisson's ratio and the incorporation into the models of the effect of the loading shoes.

The confining effect exerted by the loading shoes is evident in the three plots of Figure 8. This effect vanishes towards the centre of the panel, where stresses are more uniform. This fact highlights the need of following the prescriptions of the standards with regard to the size of the panel and length of the loading shoes. Section 4.3 investigates this effect in more detail.

Figure 8c confirms that the highest values of tensile stress appear at the centre of the panel, and are distributed on a finite region, as shown in Figure 9. This figure depicts the distribution of maximum principal stresses along the four axes of symmetry of the panel. The central fifth of the wall is subjected to tensile stresses very close to the maximum value, associated with an $\alpha_I$ of 0.48. This observation implies that the real wall of masonry would not fail at the central point of maximum tensile stresses, but at the weakest point within this central zone, considering both the high stress level and the local material properties at that specific location. As stated in Section 2, the diagonal compression test is sensitive to the local properties of the components, and the global scattering in the experimental results would reflect the variability within the constituent materials.

a)

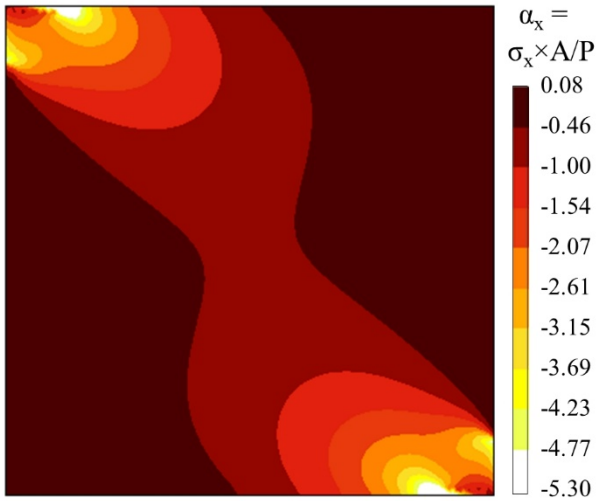


At the centre $\alpha_x = -0.56$

b)

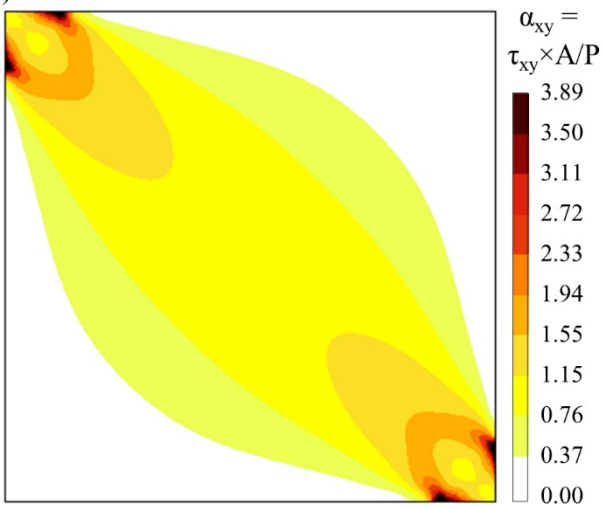


At the centre $\alpha_{xy} = 1.04$

c)

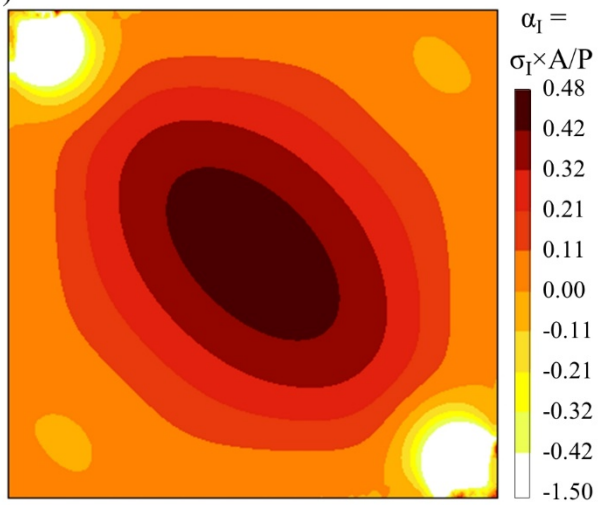


At the centre $\alpha_I = 0.48$

**Figure 8** Contour of stresses in the linear range, expressed in terms of normalized stress $\alpha$. a) Normal stresses $\sigma_x$ along X-axis [$\sigma_y$ are not shown due to the problem's symmetry], b) shear stresses $\tau_{xy}$, and c) maximum principal stresses $\sigma_I$.

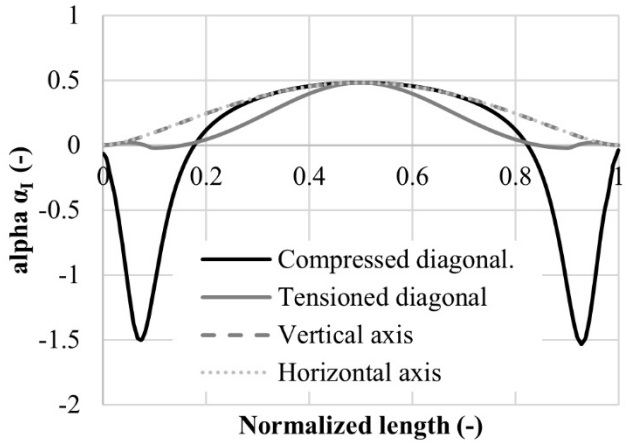


**Figure 9** Distribution of the maximum principal stresses along the axes of symmetry of the panel. Stresses are normalized and expressed in terms of the coefficient $\alpha_I$. The X-axis represents normalized lengths. The centre of the panel corresponds to the coordinate 0.5.

### 4.2.2 Non-linear range

The second stage of the study deals with the non-linear range, referring to the part of the analysis after the appearance of damage in the centre of the wall. Figure 10a shows the numerical evolution of stress components at the central element of the panel with increasing load, while Figure 10b depicts the counterpart curves in terms of coefficient $\alpha$ or normalized stresses. The horizontal axes of both figures are normalized with respect to the maximum load. The constant slope of the linear curves for the stresses agrees with the linear behaviour of the walls detected during the tests, and justifies the experimental procedure adopted herein to determine the shear modulus as a slope between load levels of 5 and 30% of the assumed maximum load. Figure 11 illustrates the tensile crack propagation in the panel with increasing load.

From Figure 10 and Figure 11, it is evident that cracking starts when the maximum principal stresses $\sigma_I$ at the centre of the panel attain the level of the input tensile strength of the material $f_t$. Reaching the level of the tensile strength triggers the apparition of damage at the centre of the panel. As shown in Figure 11, this damage develops from the central region to the corners, and eventually leads to the collapse of the panel with the formation of a complete diagonal crack. This sequence agrees

with the experimental behaviour described in Section 2. The localization of initial damage within the central region of the wall is in agreement also with the general experimental observations, as reported by different authors [4,9,12].

According to Figure 10 and Figure 11, the initiation of damage occurs at a level of applied load around 80% the maximum attained load. This value is in agreement with the observations in the experimental curves reported in Section 2. It also agrees with the results of other researches that also applied a macromodelling approach. Basili et al. [14] used a smeared crack model and the computer code MIDAS-FEA to simulate diagonal compression tests. In their analyses, the level of damage initiation was equal to 78% the maximum attained load.

This finding does not comply with the assumption of the standard [16] that establishes a correspondence between the initiation of damage at the centre of the panel and the failure of the panel. It has been found that the state of stresses of the panel at failure does not correspond to the elastic one, and that a redistribution of stresses occurs after the initiation of damage. The most important implication of this observation is that, although the failure of the panel depends on the tensile strength of the material as it triggers the damage initiation, the subsequent behaviour of the wall is more complex and it is not straightforward to identify a direct relationship between the maximum attained load $P_{max}$ and the tensile strength of the material $f_t$.

Nevertheless, the experimental outcome provided by a diagonal compression test is the maximum attained load. As mentioned in Section 2, it is difficult to precisely define in laboratory the exact moment of cracking with common instrumentation. Therefore, in order to allow the use of the diagonal compression test to determine mechanical properties of masonry, it is necessary to define a possible correlation, even if not univocal, between the maximum load and the tensile strength of the material. It is proposed to find the coefficient alpha α that correlates the maximum load with the tensile strength. For a given numerical analysis, the coefficient $\alpha_{I,calc}$ is back-calculated with Equation 20,

which involves the maximum attained load and the tensile strength used as an input parameter in the analysis:

$$\alpha_{I,calc} = \frac{f_{t,input} * A}{P_{max}} \tag{20}$$

In the three cases studied in the calibration section, the coefficient $\alpha_{I,calc}$ is almost constant. It takes the values of 0.408, 0.402 and 0.400 for the high, average and low data sets respectively. Nevertheless, those values of coefficient $\alpha_{I,calc}$ may only apply to the specific material and walls studied in the experimental campaign described in Section 2. The sensitivity of the coefficient $\alpha_{I,calc}$ to different parameters is analysed in the following Section 4.3, while its use is validated with experimental campaigns carried out by other authors in Section 4.4.

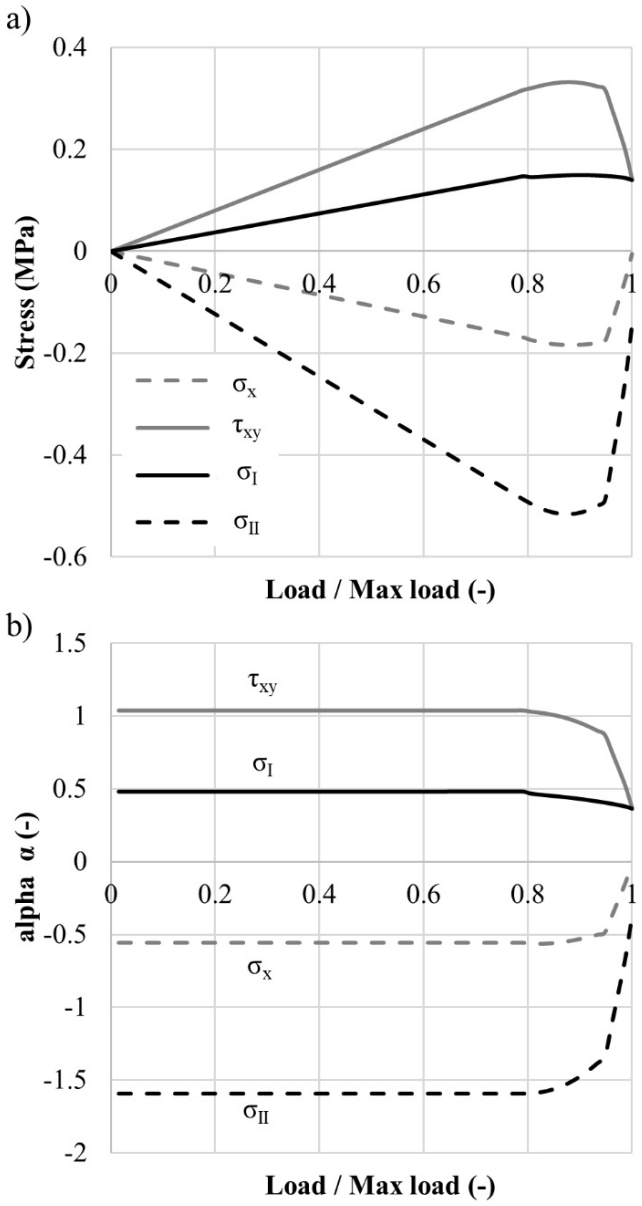


**Figure 10** a) Evolution of stresses and b) relevant normalized values $\alpha$ in the centre of the panel with increasing load. The load is normalized with respect to the maximum load attained during the analysis.

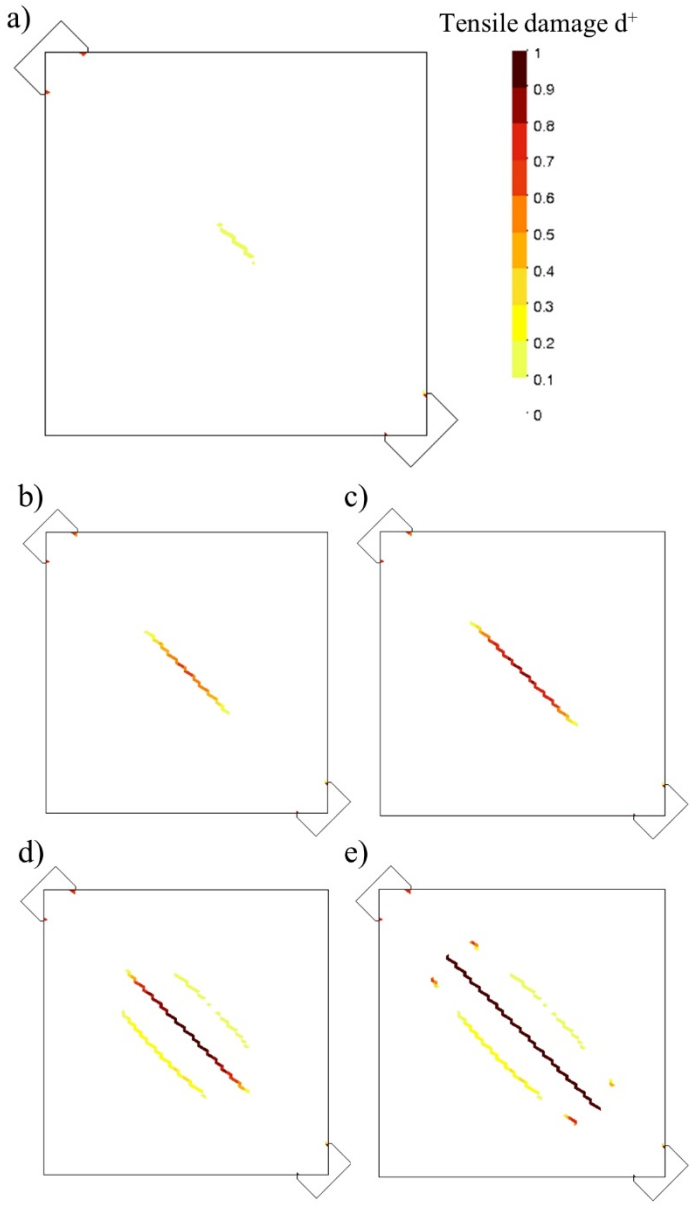


**Figure 11** Evolution of tensile damage contour for different levels of imposed displacement $\delta$. The tensile damage index $d^+$ ranges from 0 (intact material) to 1 (completely damaged material). a) $\delta$ = 0.198 mm, $P$ = 0.82$Pmax$, b) $\delta$ = 0.216 mm, $P$ = 0.89$Pmax$, c) $\delta$ = 0.230 mm, $P$ = 0.95$Pmax$, d) $\delta$ = 0.244 mm, $P$ = $Pmax$, e) $\delta$ = 0.247 mm, $P$ = 0.92$Pmax$

### 4.3 Sensitivity analysis

This section investigates the sensitivity of the back-calculated coefficient $\alpha_{I,calc}$ to different input parameters and boundary conditions. In each sensitivity analysis, the parameter investigated was varied, while the rest of properties and conditions were kept constant at the reference values. The average data set defined in the calibration Section 4.1 was taken as reference.

### 4.3.1 Material properties

Given the features of the problem, the compressive parameters, such as the compressive strength and the compressive fracture energy, have little influence in the maximum attained load and the coefficient $\alpha_{I,calc}$. The Poisson's ratio has a negligible influence as well. The material properties involved in the sensitivity analysis were the Young's modulus, the tensile strength, and the tensile fracture energy. The influence of the numerical parameter $\kappa_1$, which constitutes a special feature of the numerical model that controls the shear response, was also investigated.

Table 5 reports the values of the parameters that were considered in the sensitivity analyses. Either three or four variations were studied for each parameter, whose values were chosen as follows. The reference value for the Young's modulus, $E$ = 3477 MPa, represents a ratio of 534 with respect to the compressive strength of masonry (Table 1, $f_c$ = 6.5 MPa). As indicated by Tomazevic [84], the ratio $E$ / $f_c$ usually ranges between 200 and 1000 in common masonry. The values of Young's modulus reported in Table 5 correspond to ratios of 200, 400 and 1000. Similarly, the reference value for the tensile strength, $f_t$ = 0.155 MPa, corresponds to a ratio of 2.5% with respect to the compressive strength. Common values for the tensile strength of masonry range from 1 to 10% the compressive strength [80]. The values of tensile strength in Table 5 stand for 1%, 4% and 5% of the compressive strength. Greater percentages were considered unrealistic in this case. The choice of the values of tensile fracture energy relied on different approaches. The reference value, which allowed a good calibration in Section 4.1, was obtained by means of Equation 17 adapted in [80] from the Model Code 1990 [81]. A higher value corresponds to the unmodified expression of Model Code 1990 [81]. The lowest value corresponds to a ductility index of 0.029 mm suggested for bricks by Angelillo et al. [80]. Last, the parameter $\kappa_1$ of the constitutive model proposed by Petracca et al. [69,70] was varied within its extreme possible values, 0 and 1.

**Table 5** Values of the parameters investigated in the sensitivity analyses.

| Input parameter | $E$, Young's modulus (MPa) | $f_t$, Tensile strength (MPa) | $G_{ft}$, Tensile fracture energy (N/m) | $\kappa$1 (-) |
|---|---|---|---|---|
| *Reference value* | *3477* | *0.155* | *10.85* | *0.16* |

| | | | | |
|---|---|---|---|---|
| Variation 1 | 1302 | 0.065 | 4.73 | 0 |
| Variation 2 | 2604 | 0.26 | 18.5 | 0.1 |
| Variation 3 | 6510 | 0.325 | 56.2 | 0.3 |
| Variation 4 | - | - | - | 1 |

Figure 12 shows the results of the sensitivity analyses in terms of load – strain curves and influence on coefficient $\alpha_{I,calc}$. The effects were qualitatively predictable. Variations in the Young's modulus changed the stiffness of the curves and affected slightly the maximum attained load (Figure 12a). Variations in the tensile strength of the material were strongly related to the maximum attained load while the slope of the curves was maintained (Figure 12b). As could be expected, the influence of varying the tensile fracture energy affected mainly the post-peak range (Figure 12c). The diagonal crack has completely formed for all the cases for a strain of around 0.02%. The higher value, Gft = 56.2 N/m, gives a very ductile post-peak response in the stress-strain relationship of the constitutive model. This ductile behaviour results in a hardening response of the wall after the diagonal crack forms, which was not observed in the experiments. Finally, the variation of the parameter $\kappa_1$ shows the anticipated effect (Figure 12d): higher values correspond to higher shear capacity. It is noted that a decrease in the value of $\kappa_1$ results in an increased "weight" of the compressive surface on the constitutive shear response yielding a higher shear strength and dilatancy [69].

Quantitatively, the impact of the properties variation on the value of coefficient $\alpha_{I,calc}$ was limited, taking into account the wide range of variation investigated. In overall, the coefficient $\alpha_{I,calc}$ spanned from 0.38 to 0.45, with the exception of the highest value assigned to the tensile strength, and remained always below the value associated to the elastic response (0.48). An increase of 87% in the reference value of Young's modulus produced a decrease of only 2.5% in the coefficient $\alpha_{I,calc}$. An increase of around 420% in the reference value of tensile fracture energy involved a decrease of 5% in the coefficient $\alpha_{I,calc}$. The influence of the tensile strength was greater, as an increase of 110% in the reference value produced an increase of 16% in the value of the coefficient $\alpha_{I,calc}$. This is further evidence of the intimate relation between this parameter and the result of the diagonal compression

test. For high values of tensile strength, the load of initial damage is closer to the maximum attained load. Similarly, the parameter $\kappa_1$ influences the shear strength and results in a variation of $\alpha_{I,calc}$ equivalent to that observed for the tensile strength (see Figure 12d).

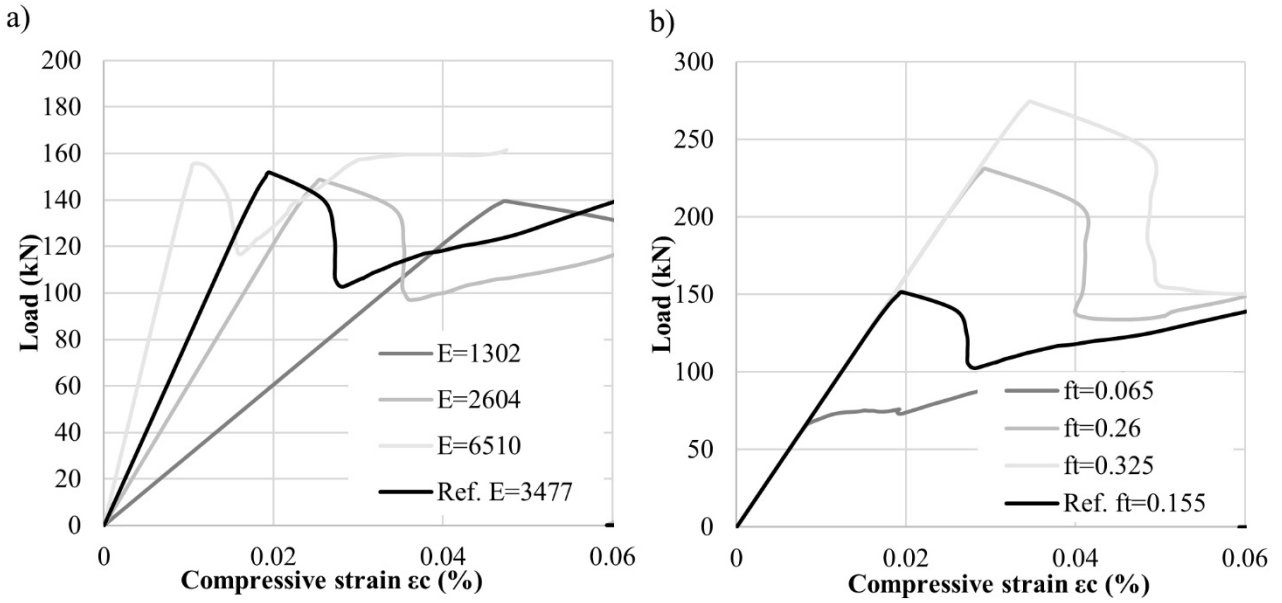


| $E$ (MPa) | 1302 | 2604 | 3477 | 6510 |
|---|---|---|---|---|
| $\alpha_{I,calc}$ | 0.437 | 0.411 | 0.402 | 0.392 |

| $f_t$ (MPa) | 0.065 | 0.155 | 0.26 | 0.325 |
|---|---|---|---|---|
| $\alpha_{I,calc}$ | 0.384 | 0.402 | 0.443 | 0.466 |

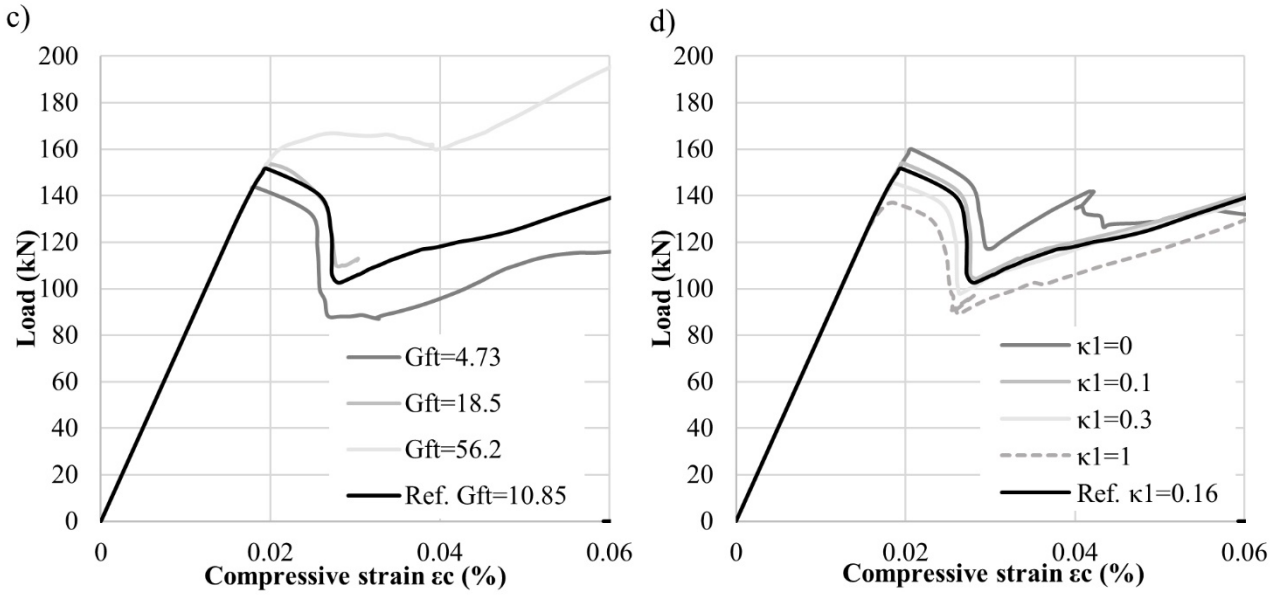


| $G_{ft}$ (N/m) | 4.73 | 10.85 | 18.5 | 56.2 |
|---|---|---|---|---|
| $\alpha_{I,calc}$ | 0.424 | 0.402 | 0.397 | 0.382 |

| $\kappa 1$ (-) | 0 | 0.1 | 0.16 | 0.3 | 1 |
|---|---|---|---|---|---|
| $\alpha_{I,calc}$ | 0.381 | 0.396 | 0.402 | 0.420 | 0.446 |

**Figure 12** Sensitivity of the model to variations of different parameters, in terms of load – strain curves and coefficient $\alpha_{I,calc}$. a) Variation of input Young's modulus, $E$. b) Variation of input tensile strength, $f_t$. c) Variation of input tensile fracture energy, $G_{ft}$. d) Variation of parameter κ1

### 4.3.2 Size and confinement effect

As mentioned in Section 2, the American standard ASTM E519 [16] and the RILEM recommendation LUMB6 [28] differ in the prescriptions of panel size and depth of the loading shoe. Although the minimum size of 1.2 m prescribed by ASTM E519 [16] is generally respected, a number of researches have considered smaller panels, mainly due to economical and practical reasons. In fact, the Chilean norm NCh 2123 [85] allows testing wallets with a minimum length of 0.6 m. Similarly, the depth of the loading shoe also presents a great variability in practice in spite of the recommendations. It is therefore necessary to investigate the effect of the size panel and the loading shoe depth on the maximum attained load and the coefficient $\alpha_{I,calc}$. A series of numerical analyses were performed with identical material properties to the average data set defined in the calibration in Section 4.1, but varying these two dimensions.

Figure 13 shows the values of the coefficient $\alpha_{I,calc}$ for the different panel sizes considered: 0.4 m, 0.6 m, 0.8 m, 1 m, 1.1 m, 1.2 m, the reference panel of 1.27 m, 1.3m, and 1.4 m. The influence of the panel size revealed to be negligible and was only significant for very small panels. A constant value of 0.4 would apply for panels from 0.6 to 1.4 m. This numerical finding is consistent with the limited experimental evidence available in literature. Knox et al. [86] did not find statistically significant differences between the strengths attained in walls 0.6 m and 1.2 m wide. In a seminal research, Fattal [87] investigated walls 1.2 m, 0.8 m, 0.6 m and 0.4 m wide. Only the smallest walls 0.4 m wide showed an evident size effect in the results.

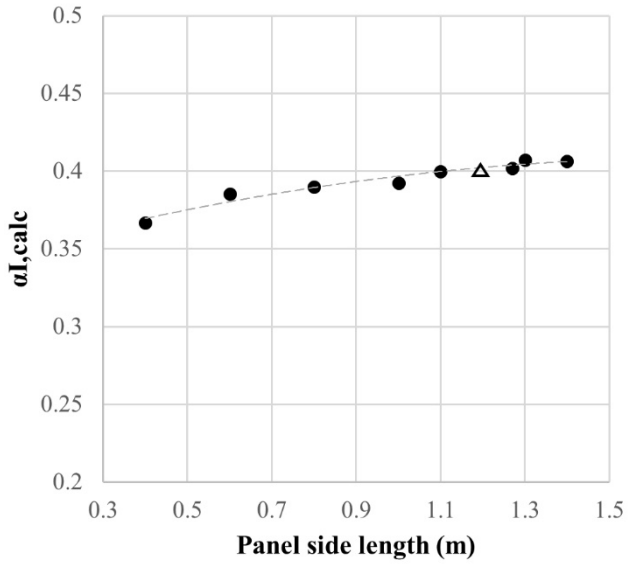


**Figure 13** Effect of the panel side length on the coefficient $\alpha_{I,calc}$. Triangle dot indicates the value corresponding to the side length recommended in ASTM E519 [16] (1200 mm).

Figure 14 illustrates the effect of the loading shoes depth on the coefficient $\alpha_{I,calc}$. With respect to the panel side length, the values investigated were 1/12$^{th}$ (0.083), 1/11$^{th}$ (0.091), 1/10$^{th}$ (0.1, as recommended by RILEM LUMB6), 1/9$^{th}$ (0.111, the reference panel), 1/8$^{th}$ (0.125, as recommended by ASTM E519), 1/7$^{th}$ (0.143), 1/6$^{th}$ (0.167), 1/4$^{th}$ (0.25), and 1/3$^{rd}$ (0.333). From 1/12$^{th}$ to 1/7$^{th}$, there was no apparent influence, and the coefficient $\alpha_{I,calc}$ remained almost constant and equal to 0.4. Conversely, the confinement exerted by the larger shoes showed to have a notable influence on the results. In the cases of 1/4$^{th}$ and 1/3$^{rd}$, the failure mode of the wall changed and a compressive strut was formed between the two loaded corners, with parallel diagonal cracks connecting the edges of the shoes. The latter are extreme cases, but may be found in practice.

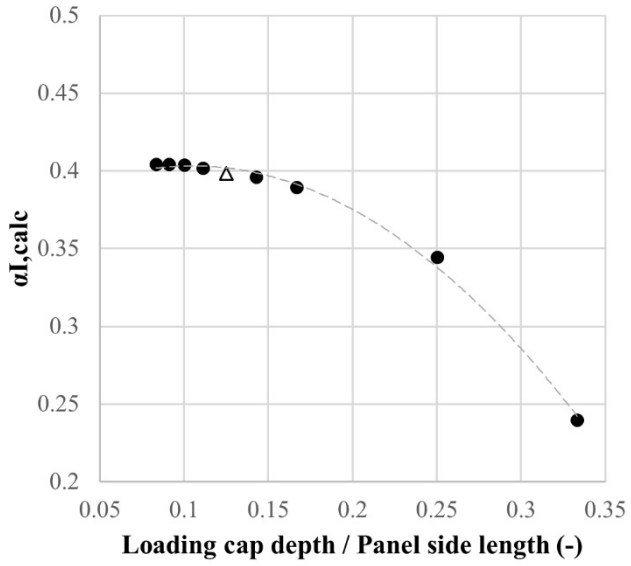


**Figure 14** Effect of the loading cap depth on the coefficient $\alpha_{I,calc}$. The X-axis indicates the loading cap depth normalized with respect to the panel side length. The triangle dot indicates the value corresponding to the ratio recommended in ASTM E519 [16] ($1/8^{th}$).

The coefficient $\alpha_{I,calc}$ has shown little sensitivity to the size and confinement effects, provided that the panel length and the loading shoes depth lay within certain limits. This conclusion may depend on the specific dimensions of the blocks and joints conforming the walls, especially on the relative dimensions of the blocks with regard to the global geometry of the wall and setup.

### 4.4 Validation

This section studies the applicability of the former findings to other masonry typologies and specimen sizes. Eight experimental campaigns carried out by other authors have been simulated [1,5,13,88–90]. These campaigns were selected under three criteria: i) They should provide sufficient and relevant information about experimental results, geometry and material properties; ii) They should present failures involving diagonal cracking; iii) They should cover a variety of typologies and sizes. The numerical simulation included the modelling of the specific geometries of the walls, and the selection of proper input material properties, according to the procedures described below. The maximum loads predicted numerically were compared to the experimental ones.

Table 6 presents the features of the eight selected campaigns. The different combinations of materials included clay bricks, concrete blocks, tuff blocks, and rubble masonry, combined with aerial lime, hydraulic lime, and cement mortars. The size of the analysed panels ranged from 0.9 to 1.63 m, and the thickness from 0.079 to 0.7 m. The input data were selected as follows. The compressive strengths $f_c$ were directly obtained from the references. The compressive fracture energies were calculated by applying the same ratio $G_{fc} / f_c$ used in this research. The Young's moduli $E$ were derived considering isotropic elasticity from the experimental shear moduli $G$, which were calculated from the experimental data by using the coefficient $\alpha_{xy}$ equal to 1.04 that has been found adequate in this research to calculate the shear stresses. In the case of the campaign by Rezaie et al.[1], the Young's modulus was directly obtained from compression tests. The values of tensile strength $f_t$ were obtained from the experimental maximum loads by means of the coefficient $\alpha_{I,calc}$ equal to 0.4 that is proposed in this study. Finally, once the tensile strengths were defined, the tensile fracture energies $G_{ft}$ were calculated by means of Equation 17.

Table 6 includes in the last three columns the comparison between the experimental maximum loads and the numerically predicted loads. Despite the great variety of the investigated geometries and materials, the average error between numerical and experimental results is 5.9%. This close estimation of the experimental capacity shows the validity of the proposed values for the coefficients $\alpha_{I,calc}$=0.4 and $\alpha_{xy}$ =1.04 to determine the tensile strength and the shear modulus of masonry from the experimental outcomes of diagonal compression tests.

The validation with campaigns carried out by other authors leads to the following remarks. First, a value of 0.4 for the coefficient $\alpha_I$ used to compute the tensile strength of masonry $f_t$ has provided good estimations of the maximum experimental loads. This value takes into consideration non-linear effects, cracking, and stress redistributions. Even if it only constitutes an approximation to the complexity of the real behaviour of masonry, it provides estimations on the safe side with respect to the elastic solution ($\alpha_I$ = 0.48) and the ASTM E519 proposal ($\alpha_I$ = 0.707). Second, the use of a

coefficient $\alpha_{xy}$ equal to 1.04 to calculate the shear stresses has led to satisfactory estimations of the shear modulus of masonry $G$. Third, Equation 17 proposed by Angelillo et al. [80] to estimate the tensile fracture energy $G_{ft}$ from the tensile strength has provided good results for this type of problem and macromodel, in which the shear response is associated with the tensile damage evolution.

**Table 6** Results from analyses of available experimental campaigns from literature. Comparison between experimental and numerically predicted maximum load.

| *Data set* | | | *Input data* | | | | | *Comparison exp - num* | | |
|---|---|---|---|---|---|---|---|---|---|---|
| *Reference* | *Typology* | *Wall size* (mm³) | $f_t$ (MPa) | $f_c$ (MPa) | $G_{ft}$ (N/m) | $G_{fc}$ (N/m) | $E$ (MPa) | $P_{exp}$ (kN) | $P_{num}$ (kN) | $\Delta_{exp\text{-}num}$ |
| Babaeidarabad et al. [88] | Clay brick + cement | 1145 × 1220 × 92 | 0.263 | 24.0 | 15.70 | 36000 | 1769 | 70.0 | 66.6 | +4.8% |
| Mahmood and Ingham [5] | Clay brick + cement lime | 1170 × 1170 × 225 | 0.054 | 5.4 | 5.18 | 8100 | 3141 | 36.0 | 40.3 | -12.0% |
| Milosevic et al. [89] | Rubble stone + air lime | 1200 × 1200 × 700 | 0.014 | 7.41 | 1.98 | 11115 | 204 | 29.0 | 29.8 | -2.6% |
| Milosevic et al. [89] | Rubble stone + hydraulic lime | 1200 × 1200 × 700 | 0.162 | 8.01 | 11.2 | 12015 | 868 | 339.0 | 303.6 | +10.4% |
| Parisi et al. [13] | Tuff block+ pozzolana | 1230 × 1230 × 310 | 0.127 | 3.96 | 9.43 | 5940 | 1100 | 121.0 | 112.1 | +7.4% |
| Rezaie et al. [1] | Rubble stone + hydraulic lime | 900 × 900 × 400 | 0.060 | 0.76 | 5.58 | 1140 | 1191 | 53.0 | 52.5 | +0.88% |
| Silva et al. [90] | Concrete block + cement | 1626 × 1626 × 79 | 0.399 | 16.8 | 21.02 | 25200 | 8600 | 128.0 | 123.8 | +3.4% |
| Silva et al. [90] | Clay brick + cement | 1219 × 1219 × 92 | 0.289 | 13.2 | 16.78 | 19800 | 2700 | 81.0 | 76.5 | +5.5% |

## 5 Conclusions

This paper has presented a combined experimental and numerical investigation on the use of the diagonal compression test to characterize the tensile strength and the shear modulus of masonry. A numerical macromodel has been calibrated with an experimental campaign that involved tests of 5 brickwork walls built in Flemish bond. The following conclusions can be drawn from the performed numerical analyses:

- In the linear range of the analyses, the numerical solution coincides qualitatively with the solution that Frocht derived theoretically for the elastic problem by photoelasticity. The numerical study shows that a wall compressed diagonally does not present a pure shear state

of stresses. The approach of ASTM E519 has shown to overestimate the maximum principal stresses ($\sigma_I = 0.707*P/A$ versus $\sigma_I = 0.48*P/A$) and to underestimate the shear stresses ($\tau_{xy} = 0.707*P/A$ versus $\tau_{xy} = 1.04*P/A$) at the centre of the panel.

- Damage initiation is triggered when the maximum principal stresses at the centre of the panel reach the masonry tensile strength. Afterwards, a redistribution of stresses takes place until the maximum load is attained and the panel fails.
- A coefficient $\alpha_I$ that correlates the maximum attained load and the input tensile strength has been back-calculated based on the numerical investigation. The tensile strength is proposed to be calculated as the maximum applied load times a coefficient $\alpha_I$ equal to 0.4, divided by the transverse area of the wall. The use of the coefficient $\alpha_I$ accounts for cracking and stress redistributions, and allows the practical use of the experimental results to determine the tensile strength of masonry. This value would be only applicable for tests that present a diagonal failure with a crack that passes by or close to the central section of the wall.
- The sensitivity of the coefficient $\alpha_I$ to the variation of several parameters has been investigated numerically. The coefficient $\alpha_I$ is sensitive to the variation of the Young's modulus and tensile strength. Its value ranges from 0.38 to 0.45, and always remains below the corresponding elastic value of 0.48.
- The coefficient $\alpha_I$ shows little sensitivity to the variation of the panel size and the size of the loading shoes, provided that these dimensions are similar to the ones suggested by the standards. The coefficient remains almost constant for walls between 0.6 m and 1.4 m wide, and for loading shoes depths spanning from $1/6^{th}$ to $1/12^{th}$ the length of the panel side.
- These findings have been validated by considering experimental results from eight campaigns carried out by other authors and available in literature. These campaigns covered a wide range of dimensions and components properties. The assumptions of a coefficient $\alpha_I$ equal to 0.4 to compute the tensile strength of masonry from the experimental maximum

load, and of a coefficient $\alpha_{xy}$ equal to 1.04 to compute the shear stresses and determine the shear modulus, allows the numerical simulations to represent correctly the experimental loads.

- The experimental campaign presented herein involving brickwork walls has shown the particularities of the Flemish bond, as the development of the diagonal cracks through both mortar joints and bricks. With the coefficients proposed in this paper, the average tensile strength of the investigated masonry is estimated equal to 0.15 MPa, while the average shear modulus is estimated equal to 1890 MPa. The compressive strengths of the component materials are 18 MPa and 2.2 MPa for bricks and mortar respectively.
- The numerical model adopted in the research, based on an ad-hoc constitutive model for masonry and a crack-tracking technique for tensile crack localization, proves to constitute a reliable tool for the assessment of masonry homogenized properties by means of comparisons with experimental results.

## Acknowledgements

The authors gratefully acknowledge the financial support from the Ministry of Science, Innovation and Universities of the Spanish Government (MCIU), the State Agency of Research (AEI), as well as that of the ERDF (European Regional Development Fund) through the project SEVERUS (Multilevel evaluation of seismic vulnerability and risk mitigation of masonry buildings in resilient historical urban centres, ref. num. RTI2018-099589-B-I00). Support from Secretaria d'Universitats i Investigació de la Generalitat de Catalunya through a predoctoral grant awarded to the first author is gratefully acknowledged.

The authors wish to thank Paolo Casadei, José Luis Sánchez and Patricio Contreras from KERAKOLL for providing part of the materials used in the experimental campaign. The authors would

like also to acknowledge Guido Camata for the fruitful discussions, and Larisa Garcia-Ramonda for the collaboration during the execution of the tests.

## References

[1] A. Rezaie, M. Godio, K. Beyer, Experimental investigation of strength, stiffness and drift capacity of rubble stone masonry walls, Constr. Build. Mater. 251 (2020) 118972. doi:10.1016/j.conbuildmat.2020.118972.

[2] N. Augenti, F. Parisi, Learning from Construction Failures due to the 2009 L'Aquila, Italy, Earthquake, J. Perform. Constr. Facil. 24 (2010) 536–555. doi:10.1061/(ASCE)CF.1943-5509.0000122.

[3] M. Tomaževič, Shear resistance of masonry walls and Eurocode 6: Shear versus tensile strength of masonry, Mater. Struct. Constr. 42 (2009) 889–907. doi:10.1617/s11527-008-9430-6.

[4] G. Magenes, G.M. Calvi, In-plane seismic response of brick masonry walls, Earthq. Eng. Struct. Dyn. 26 (1997) 1091–1112.

[5] H. Mahmood, J.M. Ingham, Diagonal Compression Testing of FRP-Retrofitted Unreinforced Clay Brick Masonry Wallettes, J. Compos. Constr. 15 (2011) 810–820. doi:10.1061/(ASCE)CC.1943-5614.0000209.

[6] V. Turnšek, F. Čačovič, Some experimental results on the strength of brick masonry walls, Proc. 2nd Int. Brick Mason. Conf. (1971) 149–156. doi:10.1111/j.1365-2664.2009.01609.x.

[7] V. Turnšek, P. Sheppard, The shear and flexural resistance of masonry walls, in: Int. Res. Conf. Earthq. Eng., 1980: pp. 517–573. doi:10.1017/CBO9781107415324.004.

[8] A.M. D'Altri, V. Sarhosis, G. Milani, J. Rots, S. Cattari, S. Lagomarsino, E. Sacco, A. Tralli, G. Castellazzi, S. de Miranda, Modeling Strategies for the Computational Analysis of Unreinforced Masonry Structures: Review and Classification, Arch. Comput. Methods Eng. (2019). doi:10.1007/s11831-019-09351-x.

[9] A. Incerti, V. Rinaldini, C. Mazzotti, The evaluation of masonry shear strength by means of different experimental techniques: A comparison between full-scale and laboratory tests, Brick Block Mason. Trends, Innov. Challenges - Proc. 16th Int. Brick Block Mason. Conf. IBMAC 2016. (2016) 1645–1652. doi:10.1201/b21889-204.

[10] P. Roca, M. Cervera, G. Gariup, L. Pelà, Structural analysis of masonry historical constructions. Classical and advanced approaches, Arch. Comput. Methods Eng. 17 (2010) 299–325. doi:10.1007/s11831-010-9046-1.

[11] L. Malyszko, In-plane shear and tensile strength test of small brickwork specimens, in: C. Modena, P.B. Lourenço, P. Roca (Eds.), Struct. Anal. Hist. Constr., 2005: pp. 291–298.

[12] C. Calderini, S. Cattari, S. Lagomarsino, The use of the diagonal compression test to identify the shear mechanical parameters of masonry, Constr. Build. Mater. 24 (2010) 677–685. doi:10.1016/j.conbuildmat.2009.11.001.

[13] F. Parisi, I. Iovinella, A. Balsamo, N. Augenti, A. Prota, In-plane behaviour of tuff masonry strengthened with

inorganic matrix-grid composites, Compos. Part B Eng. 45 (2013) 1657–1666. doi:10.1016/j.compositesb.2012.09.068.

[14] M. Basili, G. Marcari, F. Vestroni, Nonlinear analysis of masonry panels strengthened with textile reinforced mortar, Eng. Struct. 113 (2016) 245–258. doi:10.1016/j.engstruct.2015.12.021.

[15] R. Sousa, H. Sousa, J. Guedes, Diagonal compressive strength of masonry samples - Experimental and numerical approach, Mater. Struct. Constr. 46 (2013) 765–786. doi:10.1617/s11527-012-9933-z.

[16] American Society for Testing and Materials, ASTM E 519 Standard Test Method for Diagonal Tension ( Shear ) in Masonry Assemblages, (2010).

[17] N. Gattesco, I. Boem, A. Dudine, Diagonal compression tests on masonry walls strengthened with a GFRP mesh reinforced mortar coating, Bull. Earthq. Eng. 13 (2015) 1703–1726. doi:10.1007/s10518-014-9684-z.

[18] X. Wang, C.C. Lam, V.P. Iu, Comparison of different types of TRM composites for strengthening masonry panels, Constr. Build. Mater. 219 (2019) 184–194. doi:10.1016/j.conbuildmat.2019.05.179.

[19] M. Del Zoppo, M. Di Ludovico, A. Balsamo, A. Prota, In-plane shear capacity of tuff masonry walls with traditional and innovative Composite Reinforced Mortars (CRM), Constr. Build. Mater. 210 (2019) 289–300. doi:10.1016/j.conbuildmat.2019.03.133.

[20] S. Casacci, C. Gentilini, A. Di Tommaso, D. V. Oliveira, Shear strengthening of masonry wallettes resorting to structural repointing and FRCM composites, Constr. Build. Mater. 206 (2019) 19–34. doi:10.1016/j.conbuildmat.2019.02.044.

[21] L. Garcia-Ramonda, L. Pelà, P. Roca, G. Camata, In-plane shear behaviour by diagonal compression testing of brick masonry walls strengthened with basalt and steel textile reinforced mortars, Constr. Build. Mater. 240 (2020) 117905. doi:10.1016/j.conbuildmat.2019.117905.

[22] S. Chiostrini, L. Galano, A. Vignoli, On the Determination of Strength of Ancient Masonry Walls via Experimental Tests, 12th World Conf. Earthq. Eng. (2000) 1–8. http://www.iitk.ac.in/nicee/wcee/article/2564.pdf.

[23] A. Borri, G. Castori, M. Corradi, E. Speranzini, Shear behavior of unreinforced and reinforced masonry panels subjected to in situ diagonal compression tests, Constr. Build. Mater. 25 (2011) 4403–4414. doi:10.1016/j.conbuildmat.2011.01.009.

[24] M. Corradi, A. Borri, A database of the structural behavior of masonry in shear, Bull. Earthq. Eng. 16 (2018) 3905–3930. doi:10.1007/s10518-018-0328-6.

[25] European Committee for Standardization (CEN), Eurocode 8 : Design of structures for earthquake resistance — Part 3: Assessment and retrofitting of buildings, 3 (2004).

[26] FEMA/ASCE, FEMA 356. Prestandard and Commentary for the Seismic Rehabilitation of Buildings, Rehabil. Requir. (2000).

[27] Ministero delle Infrastrutture e dei Trasporti, Circolare 21 gennaio 2019 Istruzioni per l'applicazione dell' "Aggiornamento delle 'Norme techniche per le costruzioni'" di cui al decreto ministeriale 17 gennaio 2018, (2019). https://www.gazzettaufficiale.it/eli/gu/2019/02/11/35/so/5/sg/pdf.

[28] RILEM, LUMB6 Diagonal tensile strength tests of small wall specimens, (1991).

[29] M.M. Frocht, Recent advances in photoelasticity and an investigation of the stress distribution in square blocks subjected to diagonal compression, Trans. Am. Soc. Mech. Eng. 53 (1931) 135–153.

[30] F.Y. Yokel, S.G. Fattal, A failure hypothesis for masonry shearwalls, 1975.

[31] A. Brignola, S. Frumento, S. Lagomarsino, S. Podestà, Identification of Shear Parameters of Masonry Panels Through the In-Situ Diagonal Compression Test, Int. J. Archit. Herit. 3 (2008) 52–73. doi:10.1080/15583050802138634.

[32] A. Benedetti, In Plane Behaviour of Masonry Walls Reinforced with Mortar Coatings and Fibre Meshes, Int. J. Archit. Herit. 13 (2019) 1029–1041. doi:10.1080/15583058.2019.1618972.

[33] V. Alecci, M. Fagone, T. Rotunno, M. De Stefano, Shear strength of brick masonry walls assembled with different types of mortar, Constr. Build. Mater. 40 (2013) 1038–1045. doi:10.1016/j.conbuildmat.2012.11.107.

[34] P. Croce, M.L. Beconcini, P. Formichi, P. Cioni, F. Landi, C. Mochi, F. De Lellis, E. Mariotti, I. Serra, Shear modulus of masonry walls: A critical review, Procedia Struct. Integr. 11 (2018) 339–346. doi:10.1016/j.prostr.2018.11.044.

[35] G.P. Lignola, A. Bilotta, F. Ceroni, Assessment of the effect of FRCM materials on the behaviour of masonry walls by means of FE models, Eng. Struct. 184 (2019) 145–157. doi:10.1016/j.engstruct.2019.01.035.

[36] M. Del Zoppo, M. Di Ludovico, A. Prota, Analysis of FRCM and CRM parameters for the in-plane shear strengthening of different URM types, Compos. Part B Eng. 171 (2019) 20–33. doi:10.1016/j.compositesb.2019.04.020.

[37] S. Türkmen, B.T. De Vries, S.N.M. Wijte, A.T. Vermeltfoort, In-plane behaviour of clay brick masonry wallettes retrofitted with single-sided fabric-reinforced cementitious matrix and deep mounted carbon fibre strips, Bull. Earthq. Eng. 18 (2020) 725–765. doi:10.1007/s10518-019-00596-2.

[38] M. Shabdin, M. Zargaran, N.K.A. Attari, Experimental diagonal tension (shear) test of Un-Reinforced Masonry (URM) walls strengthened with textile reinforced mortar (TRM), Constr. Build. Mater. 164 (2018) 704–715. doi:10.1016/j.conbuildmat.2017.12.234.

[39] A. Incerti, A.R. Tilocca, F. Ferretti, C. Mazzotti, Influence of masonry texture on the shear strength of FRCM reinforced panels, in: R. Aguilar (Ed.), Struct. Anal. Hist. Constr., RILEM Bookseries, 2019: pp. 1623–1631. doi:10.1007/978-3-319-99441-3.

[40] European Committee for Standardization (CEN), EN 772-1:2011 Methods of Test for Masonry Units - Part 1: Determination of Compressive Strength, (2011).

[41] European Committee for Standardization (CEN), UNE-EN 772-6 Métodos de ensayo de piezas para fábrica de albañilería - Parte 6: Determinación de la resistencia a flexotracción de las piezas de hormigón de árido para fábrica de albañilería, (2002).

[42] J. Segura, D. Aponte, L. Pelà, P. Roca, Influence of recycled limestone filler additions on the mechanical behaviour of commercial premixed hydraulic lime based mortars, Constr. Build. Mater. 238 (2020) 117722. doi:10.1016/j.conbuildmat.2019.117722.

[43] European Committee for Standardization (CEN), EN 1015-11 Methods of test for mortar for masonry - Part 11: Determination of flexural and compressive strength of hardened mortar, (1999).

[44] Deutsches Institut für Normung (DIN), DIN 18555-9: Testing of mortar containing mineral binders - Part 9: Determining the compressive strength of hardened mortar, (1999).

[45] L. Pelà, A. Benedetti, D. Marastoni, Interpretation of Experimental Tests on Small Specimens of Historical Mortars, in: J. Jasienko (Ed.), Struct. Anal. Hist. Constr., DWE, 2012: pp. 716–723.

[46] D. Marastoni, L. Pelà, A. Benedetti, P. Roca, Combining Brazilian Tests on masonry cores and Double Punch Tests for the mechanical characterization of historical mortars, Constr. Build. Mater. 112 (2016) 112–127. doi:10.1016/j.conbuildmat.2016.02.168.

[47] D. Łatka, S. Serega, P. Matysek, Estimation of mortar compressive strength based on specimens extracted from masonry bed joints, in: SAHC 2018 - Struct. Anal. Hist. Constr., 2018: pp. 1949–1958. doi:10.1007/978-3-319-99441-3.

[48] D. Łatka, P. Matysek, Determination of mortar strength in historical brick masonry using the penetrometer test and double punch test, Materials (Basel). 13 (2020). doi:10.3390/ma13122873.

[49] J. Segura, L. Pelà, P. Roca, Monotonic and cyclic testing of clay brick and lime mortar masonry in compression, Constr. Build. Mater. 193 (2018) 453–466. doi:10.1016/j.conbuildmat.2018.10.198.

[50] European Committee for Standardization (CEN), EN 1052-1 Methods of test for masonry - Part 1: Determination of compressive strength, (1999).

[51] European Committee for Standardization (CEN), EN 1052-3 Methods of test for masonry - Part 3: Determination

of initial shear strength, (2007).

[52] C. Loth, Flemish bond: A hallmark of traditional architecture, Inst. Class. Archit. Art. (2011).

[53] T. Li, N. Galati, J.G. Tumialan, A. Nanni, Analysis of unreinforced masonry concrete walls strengthened with glass fiber-reinforced polymer bars, ACI Struct. J. 102 (2005) 569–577. doi:10.14359/14561.

[54] N. Ismail, R.B. Petersen, M.J. Masia, J.M. Ingham, Diagonal shear behaviour of unreinforced masonry wallettes strengthened using twisted steel bars, Constr. Build. Mater. 25 (2011) 4386–4393. doi:10.1016/j.conbuildmat.2011.04.063.

[55] European Committee for Standardization (CEN), EN 12390-13 Testing hardened concrete - Part 13: Determination of secant modulus of elasticity in compression, (2013).

[56] American Society for Testing and Materials, ASTM E111 Standard Test Method for Young's Modulus , Tangent Modulus , and Chord Modulus, (2010). doi:10.1520/E0111-04R10.

[57] L. Garcia-Ramonda, Seismic retrofit of masonry with innovative materials for strengthening and repair, PhD Thesis, Universitat Politècnica de Catalunya, 2020.

[58] A. Borri, M. Corradi, G. Castori, A. De Maria, A method for the analysis and classification of historic masonry, Bull. Earthq. Eng. 13 (2015) 2647–2665. doi:10.1007/s10518-015-9731-4.

[59] V. Alecci, S. Barducci, A. D'Ambrisi, M. De Stefano, F. Focacci, R. Luciano, R. Penna, Shear capacity of masonry panels repaired with composite materials: Experimental and analytical investigations, Compos. Part B Eng. 171 (2019) 61–69. doi:10.1016/j.compositesb.2019.04.013.

[60] W.S. Lei, A generalized weakest-link model for size effect on strength of quasi-brittle materials, J. Mater. Sci. 53 (2018) 1227–1245. doi:10.1007/s10853-017-1574-8.

[61] J. Milosevic, M. Lopes, A.S. Gago, R. Bento, Testing and modeling the diagonal tension strength of rubble stone masonry panels, Eng. Struct. 52 (2013) 581–591. doi:10.1016/j.engstruct.2013.03.019.

[62] A. Borri, G. Castori, M. Corradi, Determination of Shear Strength of Masonry Panels Through Different Tests, Int. J. Archit. Herit. 9 (2015) 913–927. doi:10.1080/15583058.2013.804607.

[63] F. Parisi, C. Balestrieri, D. Asprone, Nonlinear micromechanical model for tuff stone masonry: Experimental validation and performance limit states, Constr. Build. Mater. 105 (2016) 165–175. doi:10.1016/j.conbuildmat.2015.12.078.

[64] A. Gabor, E. Ferrier, E. Jacquelin, P. Hamelin, Analysis and modelling of the in-plane shear behaviour of hollow brick masonry panels, Constr. Build. Mater. 20 (2006) 308–321. doi:10.1016/j.conbuildmat.2005.01.032.

[65] C. Chisari, L. Macorini, C. Amadio, B.A. Izzuddin, Identification of mesoscale model parameters for brick-

masonry, Int. J. Solids Struct. 146 (2018) 224–240. doi:10.1016/j.ijsolstr.2018.04.003.

[66] S. Zhang, S.M. Taheri Mousavi, N. Richart, J.F. Molinari, K. Beyer, Micro-mechanical finite element modeling of diagonal compression test for historical stone masonry structure, Int. J. Solids Struct. 112 (2017) 122–132. doi:10.1016/j.ijsolstr.2017.02.014.

[67] R. Faria, J. Oliver, A rate dependent plastic-damage constitutive model for large scale computations in concrete structures, CIMNE, 1993.

[68] S. Saloustros, M. Cervera, L. Pelà, Tracking multi-directional intersecting cracks in numerical modelling of masonry shear walls under cyclic loading, Meccanica. 53 (2018) 1757–1776. doi:10.1007/s11012-017-0712-3.

[69] M. Petracca, L. Pelà, R. Rossi, S. Oller, G. Camata, E. Spacone, Regularization of first order computational homogenization for multiscale analysis of masonry structures, Comput. Mech. 57 (2016) 257–276. doi:10.1007/s00466-015-1230-6.

[70] M. Petracca, L. Pelà, R. Rossi, S. Zaghi, G. Camata, E. Spacone, Micro-scale continuous and discrete numerical models for nonlinear analysis of masonry shear walls, Constr. Build. Mater. 149 (2017) 296–314. doi:10.1016/j.conbuildmat.2017.05.130.

[71] J. Lubliner, J. Oliver, S. Oller, E. Oñate, A plastic-damage model for concrete, Int. J. Solids Struct. 26 (1989) 252. doi:10.1016/0148-9062(89)91126-1.

[72] M. Cervera, C. Agelet de Saracibar, M. Chiumenti, COMET - Data input manual version 5.0. Technical Report IT-308, Barcelona, 2002.

[73] S. Saloustros, M. Cervera, L. Pelà, Challenges, Tools and Applications of Tracking Algorithms in the Numerical Modelling of Cracks in Concrete and Masonry Structures, Arch. Comput. Methods Eng. 26 (2019) 961–1005. doi:10.1007/s11831-018-9274-3.

[74] R. Clemente, Análisis estructural de edificios históricos mediante modelos localizados de fisuración, PhD Thesis, Universitat Politècnica de Catalunya, 2006.

[75] L. Pelà, M. Cervera, P. Roca, Continuum damage model for orthotropic materials: Application to masonry, Comput. Methods Appl. Mech. Eng. 200 (2011) 917–930. doi:10.1016/j.cma.2010.11.010.

[76] L. Pelà, Continuum damage model for nonlinear analysis of masonry structures, PhD Thesis, Universitat Politècnica de Catalunya, 2009.

[77] S. Saloustros, L. Pelà, M. Cervera, P. Roca, Finite element modelling of internal and multiple localized cracks, Comput. Mech. 59 (2017) 299–316. doi:10.1007/s00466-016-1351-6.

[78] COMET, Coupled Mechanical and Thermal analysis, (2016). https://www.cimne.com/comet.

[79] GiD v.14, The personal pre- and post-processor, (2018). https://www.gidhome.com/.

[80] M. Angelillo, P.B. Lourenço, G. Milani, Masonry behaviour and modelling, in: Mech. Mason. Struct., Springer, 2014. doi:10.1007/978-3-7091-1774-3.

[81] CEB-FIP, Model Code 1990, (1993).

[82] CEB-FIP, Model Code 2010, (2012).

[83] M. Petracca, L. Pelà, R. Rossi, S. Oller, G. Camata, E. Spacone, Multiscale computational first order homogenization of thick shells for the analysis of out-of-plane loaded masonry walls, Comput. Methods Appl. Mech. Eng. 315 (2017) 273–301. doi:10.1016/j.cma.2016.10.046.

[84] M. Tomazevic, Earthquake-resistant design of masonry buildings, Imperial College Press, 1999. doi:https://doi.org/10.1142/p055.

[85] I.N. de Normalización, NCh 2123 Albañilería confinada. Requisitos de diseño y cálculo, (2003).

[86] C.L. Knox, D. Dizhur, J.M. Ingham, Experimental study on scale effects in clay brick masonry prisms and wall panels investigating compression and shear related properties, Constr. Build. Mater. 163 (2018) 706–713. doi:10.1016/j.conbuildmat.2017.12.149.

[87] S.G. Fattal, The capacity of unreinforced masonry shear walls under membrane loads, in: Earthq. Resist. Mason. Constr. Natl. Work., 1977: pp. 177–197.

[88] S. Babaeidarabad, F. De Caso, A. Nanni, URM walls strengthened with fabric-reinforced cementitious matrix composite subjected to diagonal compression, J. Compos. Constr. 18 (2014). doi:10.1061/(ASCE)CC.1943-5614.0000441.

[89] J. Milosevic, A.S. Gago, M. Lopes, R. Bento, Experimental assessment of shear strength parameters on rubble stone masonry specimens, Constr. Build. Mater. 47 (2013) 1372–1380. doi:10.1016/j.conbuildmat.2013.06.036.

[90] P.F. Silva, P. Yu, A. Nanni, Monte Carlo simulation of shear capacity of URM walls retrofitted by polyurea reinforced GFRP grids, J. Compos. Constr. 12 (2008) 405–415. doi:10.1061/(ASCE)1090-0268(2008)12:4(405).